IDA

INSTITUTE FOR DEFENSE ANALYSES

Double Negative Materials (DNM), Phenomena and Applications

John Franklin
John Biddle
Bohdan Balko

July 2009

IDA Document D-3887
Log: H 09-000915

This work was conducted under IDA's central research program, CRP 2117. The publication of this IDA document does not indicate endorsement by the Department of Defense, nor should the contents be construed as reflecting the official position of that Agency.

INSTITUTE FOR DEFENSE ANALYSES

IDA Document D-3887

Double Negative Materials (DNM), Phenomena and Applications

John Franklin
John Biddle
Bohdan Balko

Preface

This work was supported by a Central Research Program (CRP) task at the Institute for Defense Analyses (IDA).

Foreword

When we started the work on this document in Fiscal Year (FY) 2006, the double negative materials (DNMs) or negative index of refraction (NIR) materials research community was involved in justifying basic physical questions of causality, validity of the concept of negative index of refraction interpretation of experimental results, and so forth. At the same time, progress was being made in developing different ways of constructing DNMs, increasing the range of frequencies toward the optical/visible regime, approaching three-dimensional (3D) operability, reducing attenuation, and widening the frequency window. However, even now in 2009, questions about the validity of the DNM concept are still being challenged.[1] All this has been going on while practical applications are moving forward and new designs of metamaterial structures are being introduced and tested.

As a result of this study, new areas of interest to IDA opened: (1) superlenses or beating the diffraction limit, (2) reverse Casimir effect for reducing friction/stiction in microelectromechanical systems (MEMS), (3) cloaking in two and three dimensions, and (4) the development of transformation optics. We believe that these new areas of interest are worthy of investigation by the Department of Defense (DoD).

---

1 Munk, B. A. *Metamaterials: Critique and Alternatives* (New York: John Wiley and Sons, 2009).

Contents

Executive Summary ES-1

1. Introduction 1-1

   1.1. Double Negative Material (DNM)—What is it? 1-1
   1.2. Early History 1-4
   1.3 Recent History 1-4
   1.4 Trends 1-5
   1.5 Supplementary Material 1-5

2. Background 2-1

   2.1. Maxwell's Equations 2-2
   2.2. Possible Combinations of ε and μ in Materials 2-4

3. Basic Physics Phenomena 3-1

   3.1. Radiating Dipole 3-1
   3.2. Resonances in Materials (Forced Oscillations – Mass on a Spring) 3-2
   3.3 Calculation of the Index of Refraction: Transport Through a Plate 3-4

4. New Phenomena and Applications—or What Can We Do Now That We Could Not Do Before? 4-1

   4.1. Reverse Cerenkov Radiation 4-2
   4.2. Reverse Doppler Effect 4-4
   4.3 Reverse Casimir Effect 4-5
   4.4 Reverse Snell's Law 4-6
   4.5 Metamaterials as a Perfect Lens 4-7
   4.6 Cloaking/Invisibility 4-10

5. Manufacturing a DNM 5-1

Glossary GL-1

Appendixes

A. October 2008 Briefing: Double Negative Materials (DNMs) A-1
B. Glossary for Double Negative Materials (DNMs) B-1
C. Bibliography for Double Negative Materials (DNMs) C-1
D. Computer Model of Electromagnetic (EM) Propagation in Double Negative Materials (DNMs) D-1
E. Modeling Double Negative Materials (DNMs) E-1
F. Metamaterial Applications F-1

Figures

1-1. EM Fields in a Plane Propagating Wave 1-1

1-2. Orientation of Vectors in Positive Index of Refraction (PIR) Material and DNM 1-2

1-3. Refraction in Normal Material (Blue Line) and DNM (Red Line) 1-3

1-4. Effect on EM Beams of Lenses Made From (a) Normal Material and (b) DNM 1-3

1-5. Effect on EM Beams of Plane Plates Made From (a) Normal Material and (b) DNM 1-4

1-6. First Experimental Evidence for DNM 1-5

1-7. Number of Citations of Veselago's Seminal Paper on DNM 1-6

1-8. Papers on DNM From 1990 to 2006 1-6

2-1. An EM Beam Interacting With Four Possible Materials 2-5

2-2. EM Spectrum Showing Frequency Windows for Potential Location of Negative μ and ε in Natural Materials 2-6

3-1. Electric Dipole Radiation Pattern 3-1

3-2. Mass on a Spring Attached to a Wall 3-2

3-3. Absorptive (Blue) and Dispersive (Green) Amplitudes (Real and Imaginary Components in Some Developments Using Complex Notation) for the Response From a Forced Harmonic System 3-3

3-4. Transport of EM Radiation Through a Material Showing the Source (*S*), a dipole Absorber/Emitter in the Material, and an External Point (*P*) at Which the Field Is Recorded 3-5

4-1. Wave Fronts for Charged Particles Moving (a) Slower and (b) Faster Than the Speed of Light in a Normal Material 4-2

4-2. Polarization of Molecules in Normal Media for the Two Cases Shown in Figure 4-1(a) and 4-1(b) 4-3

4-3. Geometry of Normal Cerenkov Radiation 4-3

4-4. (a) Normal Cerenkov Wave and (b) Reverse Cerenkov Wave Due To Transport Through a DNM 4-4

4-5. Doppler Effect on Receding Boundary 4-4

4-6 Difference in Vacuum Fluctuations Between Plates and an External Region for Normal Materials 4-5

4-7. Simple Illustration of Perfect Lensing 4-8

4-8. An Artist's Rendition of EM Waves Traveling Around an Enclosed Space 4-10

5-1. Wire Structure 5-1

5-2. (a) Plan View of a Split Ring Showing Definitions of Distances; (b) Sequence of Split Rings Shown in Their Tracking Sequence 5-2

5-3. Plan View of a Split-Ring Structure in a Square Array (Lattice Spacing "*a*") 5-2

5-4. Constructing an Isotropic Material 5-3

5-5. Wire and Split-Ring Structure Designed for the Megahertz Range 5-3

5-6. Boeing Cube Structure Designed for the Gigahertz Range 5-4

5-7. Wire and Split-Ring Structures for Higher Frequencies 5-4

5-8. Fishnet Structures for Higher Frequencies 5-5

5-9. Trends in the Development of Metamaterials From Split Rings to Wire-Mesh Fishnet to Dielectric Nanoparticles 5-6

Executive Summary

In this report, we will discuss the nature of negative index of refraction (NIR) materials or double negative materials (DNMs), their realization (i.e., how they are produced), their special effects and potential applications, and their modeling—starting with simple basic models and culminating with complex computer codes.

"Normal" optical materials that have electric permeability $\varepsilon > 0$ and magnetic permittivity $\mu > 0$ are quite familiar to students of physics and engineering. DNMs that have electric permeability $\varepsilon < 0$ and magnetic permittivity $\mu < 0$ are quite different. They do not normally occur in nature, are man-made, and have some unusual properties. The purpose of this paper is to explore this second possibility.

DNM or left-handed material (LHM), although the subject of much speculation in 1964, was not fabricated until the year 2000 (at a narrow bandwidth centered around 4.84 GHz). The term "metamaterial" was used by the Defense Advanced Research Projects Agency (DARPA)[2] for these new materials. These materials are constructed from normal materials (e.g., copper) in such a way that they act as scattering centers with special properties for affecting electric and magnetic fields. The novel bulk electromagnetic (EM) properties emerge from the collective response of subwavelength structures made out of the normal structures. Since the year 2000, many other DNM have been constructed using various techniques and pushing the operational region into higher frequencies, including the visible.

---

[2] In 2001, the Defense Advanced Research Projects Agency/Defense Sciences Office (DARPA/DSO) set up a metamaterials research program. DARPA's initial interest was in applications beyond optics, such as magnets for more powerful motors, radar applications, and textured surfaces that could control a material's heat-handling capabilities. DARPA later extended its interest to advances in ultra-high-frequency antennas for possible radar applications.

1. Introduction

1.1 Double Negative Material (DNM)—What Is It?

Recently, much interest has been focused on metamaterials that show unusual interactions with electromagnetic (EM) waves—interactions that have not been seen before with normal, naturally occurring materials. These materials have been referred to as negative group velocity (NGV) materials, negative index materials (NIMs), double negative materials (DNMs), left-handed materials (LHMs), and negative index of refraction (NIR) materials. All these names are appropriate, but, in this paper, DNM will be used most often.

EM waves in space contain an electric field (E) and a magnetic field (H) perpendicular to the direction of propagation, ***k,*** as shown in Figure 1-1.

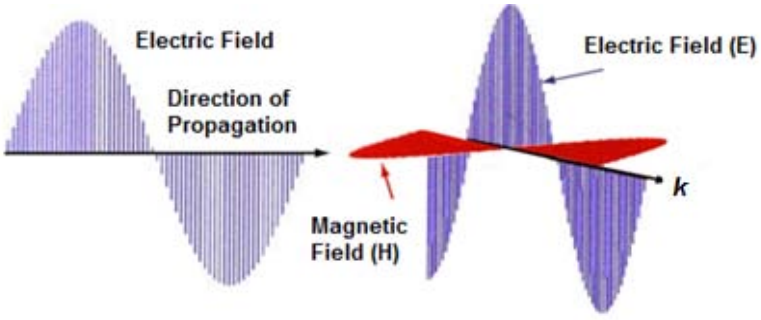

Figure 1-1. EM Fields in a Plane Propagating Wave

Propagation of EM waves is described in terms of the phase velocity, given by $v_p = \frac{\lambda}{T}$, where λ is the wavelength and T is the period of the wave, and the group velocity, given by $v_g = \frac{\partial \omega}{\partial k}$, where ω is the frequency of the wave and k is its wave number.[3] The energy flow in space is given by Poynting's vector, $\boldsymbol{S} = \boldsymbol{E} \times \boldsymbol{H}$. The two velocities describe two different properties of a wave: the phase velocity, $\boldsymbol{v_p}$, with which the phase of a wave of one frequency travels and the group velocity, $\boldsymbol{v_g}$, with which the envelope

[3] Sometimes the parameters v_p, v_g, and k will be bolded to indicate that they are vectors and have a direction associated with them.

of the wave propagates and, in most cases, can be thought of as the velocity of energy transfer.

Figure 1-2 shows the difference between group and phase velocity in normal materials (i.e., right handed materials (RHMs)) and DNMs or LHMs).

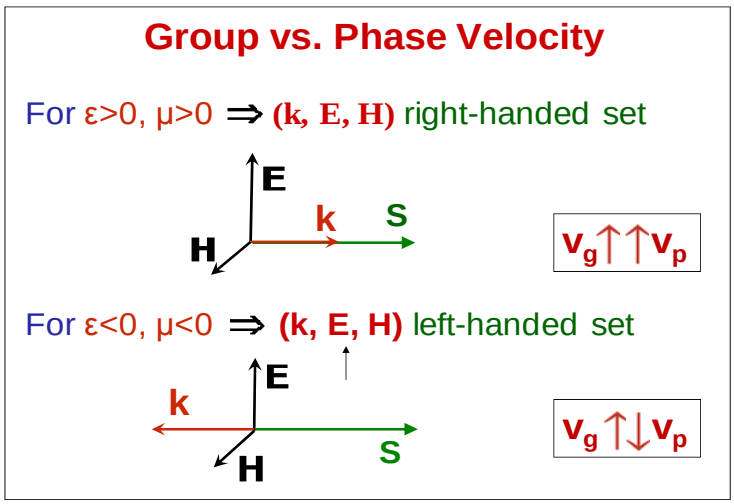

Figure 1-2. Orientation of Vectors in Positive Index of Refraction (PIR) Material and DNM

Note 1 for Figure 1-2: *In the figure, u is the energy density, $\boldsymbol{v}_g$ is the group velocity, and $\boldsymbol{v}_p$ is the phase velocity. $\boldsymbol{v}_g$ is parallel to $\boldsymbol{S}$, and $\boldsymbol{v}_p$ is parallel to $\boldsymbol{k}$.*

Note 2 for Figure 1-2: $\boldsymbol{k} \times \boldsymbol{E} = \omega \mu \boldsymbol{H}$, *and* $\boldsymbol{S} = \boldsymbol{E} \times \boldsymbol{H} = \langle u \rangle \boldsymbol{v}_g$.

The simplest example of the difference between normal materials and DNMs is obtained by comparing the effects of the two materials on refraction. In a normal transparent (dielectric) material, an EM beam is refracted toward the normal (blue line) as it passes from air into the higher optical density (positive index) material as shown in Figure 1-3. In a DNM, the beam is refracted to the other side (red line) of the normal as shown in Figure 1-3.

The angle of refraction is obtained from Snell's law, which states that the ratio of the sines of the angles of incidence and refraction is equal to the ratio of velocities in the two media or, equivalently, to the inverse ratio of the indexes of refraction n_1 and n_2. Thus,

$$n_1 \sin(\theta_1) = n_2 \sin(\theta_2), \tag{1.1}$$

where θ_1 and θ_2 are the angles of incidence and refraction respectively, as shown in Figure 1-3. For a DNM, the law still holds. Since $n_2' < 0$, and $\theta_2' < 0$, the product $n_2' \sin(\theta_2')$ is positive, but the refracted beam direction is to the left since $\theta_2' < 0$, as shown in Figure 1-3.

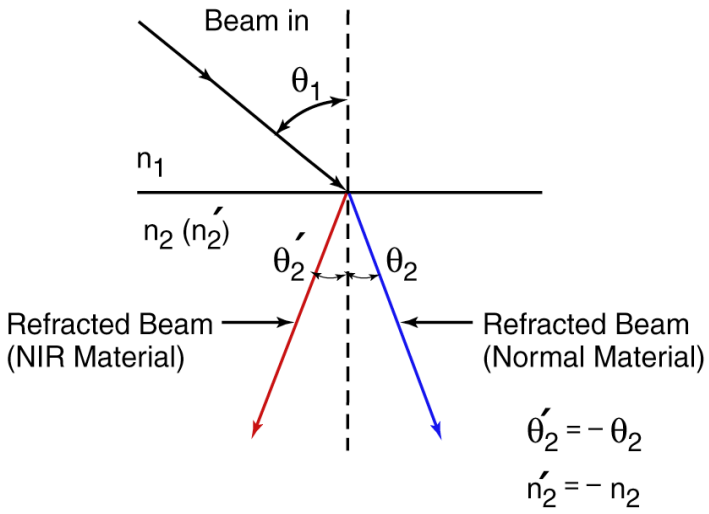

Figure 1-3. Refraction in Normal Material (Blue Line) and DNM (Red Line)

Figure 1-4 shows the practical application of this DNM. In this figure, we compare the effects of focusing the light of lenses made from normal (blue) and DNM (red). Notice that the DNM has the opposite effect from that of the normal material: convex lenses diverge the beam while concave lenses converge the beam. In Figure 1-5, a plate containing normal material (a) diverges the beam (s1) so that a virtual source is seen inside the material and a plate containing DNM (b) focuses the beam (s1) inside the material (f1) and on the other side from the source outside the material (f2).

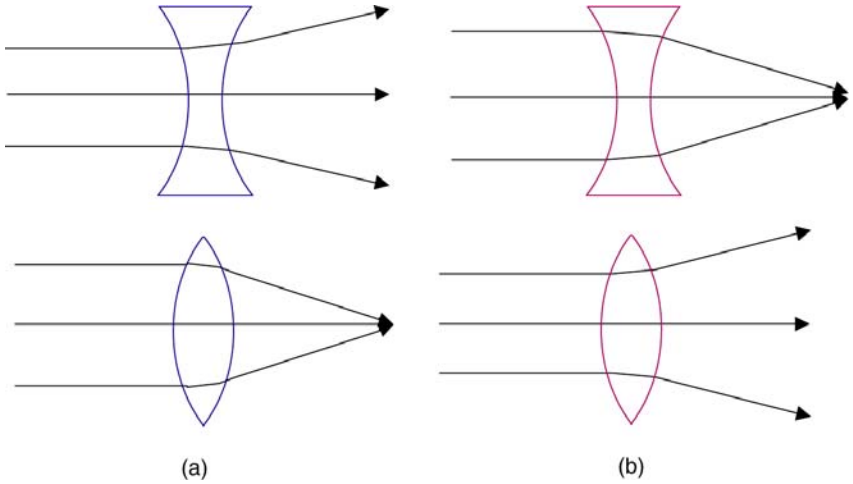

Figure 1-4. Effect on EM Beams of Lenses Made From (a) Normal Material and (b) DNM

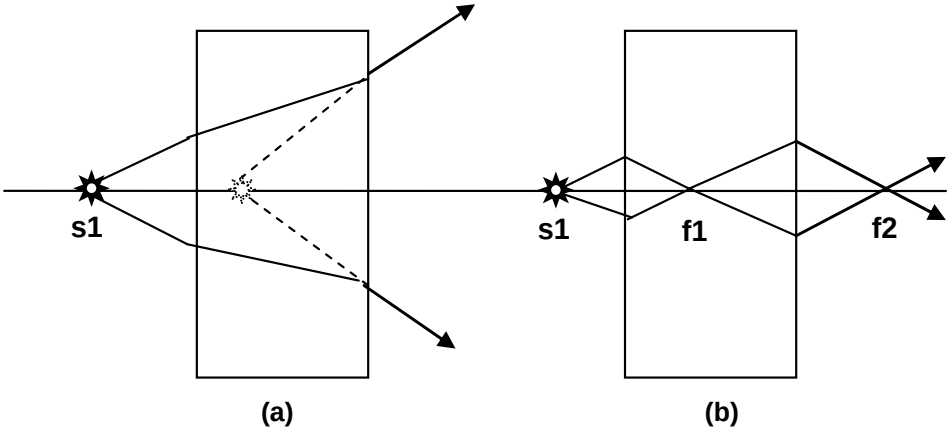

Figure 1-5. Effect on EM Beams of Plane Plates Made From (a) Normal Material and (b) DNM

1.2 Early History

Most authors attribute the first theoretical study of DNM to V. G. Veselago (1967), who developed the basic theoretical underpinnings of the interaction of EM waves with these materials and discussed various unusual effects on well-known phenomena such as refraction, Snell's law of refraction, the Doppler Effect, Cherenkov radiation, and so forth. Others preceded him in considering the idea—if not for electromagnetism, then for acoustics: D. V. Sivukhin (1957); G.D. Malyuzhinets (1957); L.I. Mandel'shtam (1950); H. C. Pocklington (1905); and H. Lamb (1905), who may have been the first to suggest backward waves in mechanical systems. However, Veselago provided a theoretical paper that had the first serious and complete discussion of DNM.[4]

1.3 Recent History

Whereas the early history concentrated on the theoretical analysis of various effects within the realm of physical possibility, recent history has been concerned with experimental developments: construction of DNMs (metamaterials), testing, and the search for useful applications. This new focus does not mean that theoretical studies have been abandoned—only that the focus is on applications since the validity of the phenomena has been well established. The experimental verification of the phenomena by R. A. Shelby, D. R. Smith, and S. Schultz in 2001 and Andrew A. Houck, J. B. Brock, and I. L.

---

4 Veselago, V. G. "The Electrodynamics of Substances With Simultaneously Negative Values of ε and μ." *Soviet Physics Uspekhi* 10 (4) (January–February 1968): 509–514. Available at http://www.iop.org/EJ/article/0038-5670/10/4/R04/PHU_10_4_R04.pdf?request-id=be94154d-cd29-4796-aca6-209e7c9b79bb

Chuang in 2003 established this trend. The first experimental evidence for DNM is shown in Figure 1-6. The experiment was performed at 100 MHz, with two prisms (one made of Teflon (normal material) and the other made of a DNM (i.e., LHM)). The Teflon beam is refracted at 30 deg while the LHM material refracts at a negative angle (in this case, –60 deg), as was expected with a DNM.

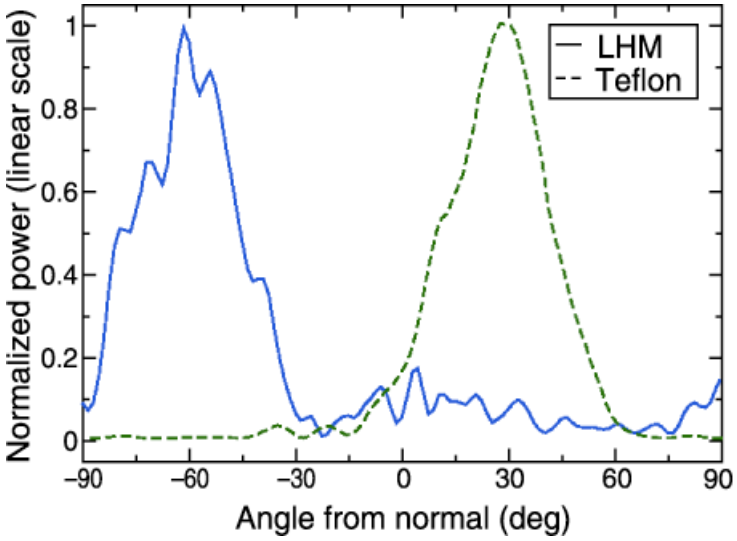

Figure 1-6. First Experimental Evidence for DNM

Source: Shelby, R. A., D. R. Smith, and S. Schultz. April 6, 2001. **"**Experimental verification of a Negative Index of Refraction." *Science* 292 (5514): 77–79.

Note1 for Figure 1-6: *DNM result solid (blue line) line; normal material dashed line (green line).*

Note 2 for Figure 1-6: *The LHM consist of square copper split ring resonators and copper wire strips on fiberglass circuit board material. The rings and wires are on opposite sides of the boards, and the boards have been cut and assembled into an interlocking lattice. The LHM had a unit cell dimension of 5 mm, a factor of 6 smaller than the X-band (8 to 12 GHz) center wavelength of 3 cm.*

1.4 Trends

The chart in Figure 1-7 shows the number of citations in the literature to Veselago's seminal paper on DNM from 2000 to 2003. In Figure 1-8, we show the number of publications on LHMs from 1990 to 2006 obtained by a "Google Scholar" search.

1.5 Supplementary Material

Appendix A, which is on a compact disk (CD) attached to the inside back cover of this document, is a briefing on DNMs that was presented in October 2008. This briefing contains movie clips (pages A-7, A-29, and A-30) that show a simulation of EM waves propagating through normal material and through DNM.

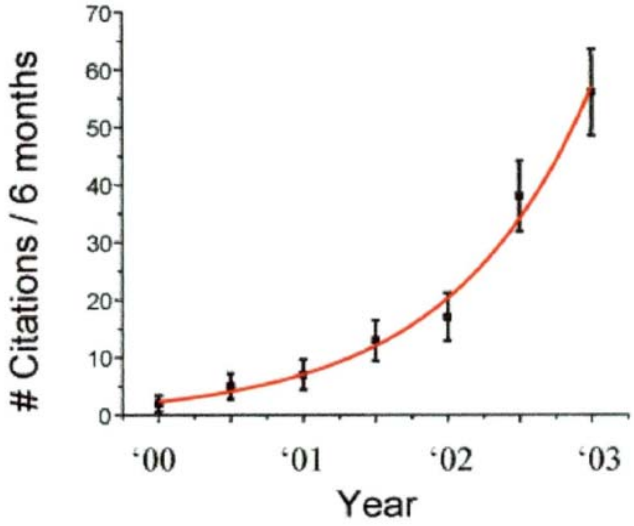

Figure 1-7. Number of Citations of Veselago's Seminal Paper on DNM

Source: MITRE Corporation. November 2003. *JASON Report on Metamaterials.* MITRE Technical Report 03-510. McLean, VA. MITRE Corporation.

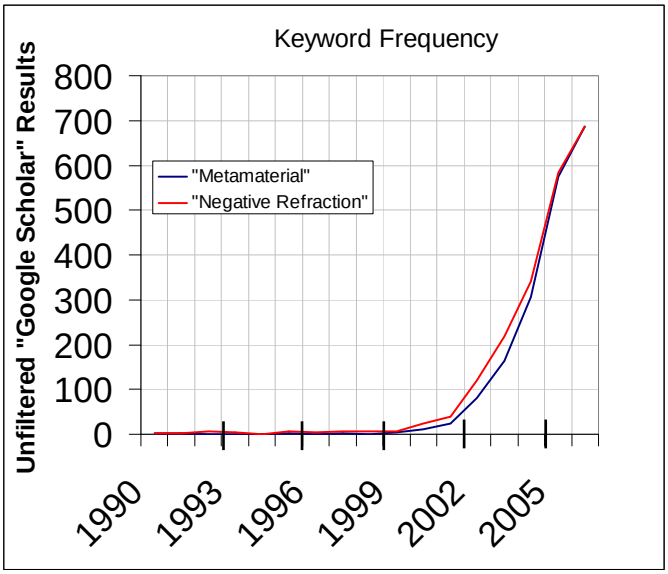

Figure 1-8. Papers on DNM From 1990 to 2006

2. Background

To understand the DNM phenomena and the excitement it is causing and to appreciate the many new applications that researchers are considering, we need to examine the response functions of materials to EM fields. To help supplement this investigation, Appendix B presents a glossary of terms used in DNM discussions, and Appendix C contains a bibliography of DNM.

Two macroscopic parameters that describe materials and their interaction with EM fields are the electric permittivity, ε, and the magnetic permeability, μ. The parameter ε determines how well a material polarizes—or creates an electric dipole, $\boldsymbol{P}$. The permittivity defines the displacement $\boldsymbol{D} = \varepsilon\boldsymbol{E} = \varepsilon_0\boldsymbol{E} + \boldsymbol{P}$. The parameter μ determines how well a material magnetizes—or creates a magnetic dipole, M—and defines the magnetization $\boldsymbol{H} = \boldsymbol{B}/\mu$ or $\boldsymbol{B} = \mu\boldsymbol{H} = \mu_0\boldsymbol{H} + \boldsymbol{M}$.

The index of refraction, n, is usually calculated as the product $(\mu\varepsilon)^{1/2}$. For negative μ and ε, a simple replacement of μ with $-\mu$ and ε with $-\varepsilon$ still gives a positive value for the index of refraction since $n = ((-\mu)(-\varepsilon))^{1/2} = (\mu\varepsilon)^{1/2}$ is still positive. However, the square root has two solutions: one positive and one negative. Thus, the simple solution when μ and ε are both negative, is to take the negative square root to get the index of refraction:

$$n = (\pm)\,(\mu\varepsilon)^{1/2} \text{ (so pick } n = (-)(\mu\varepsilon)^{1/2}). \tag{2.1}$$

However, we have a more satisfactory solution in complex space. Using complex notation, the result comes out more naturally with $-\mu$ expressed as $\mu\, e^{i\pi}$ and $-\varepsilon$ expressed as $\varepsilon\, e^{i\pi}$, so that $n = [(-\mu)(-\varepsilon)]^{1/2}\,(\mu\, e^{i\pi}\,\varepsilon\, e^{i\pi})^{1/2} = (\mu\,\varepsilon)^{1/2}\, e^{i\pi} = -(\mu\varepsilon)^{1/2}$.

An EM wave propagating through a medium is characterized by its wave velocity and group velocity and its interaction with the material through material properties μ and ε. The relationship between the wave vector $\boldsymbol{k}$ and the vectors $\boldsymbol{E}$ and $\boldsymbol{H}$ is given by

$$\boldsymbol{k} \times \boldsymbol{E} = \omega\, \mu\boldsymbol{H} \tag{2.2}$$

for a sinusoidal wave of frequency ω.

The Poynting vector, $\boldsymbol{S}$, represents energy flow and is given by

$$\boldsymbol{S} = \boldsymbol{E} \times \boldsymbol{H} = \frac{1}{\mu_0} \boldsymbol{E} \times \boldsymbol{B} = \langle u \rangle \boldsymbol{v_g}, \tag{2.3}$$

where u is the energy per volume and $\boldsymbol{v_g}$ the group velocity.

Figure 1-1 shows the difference between group and phase velocity in normal materials (i.e., RHMs) and DNM or LHMs. How an EM beam propagates through a material and how it passes through an interface between two materials of different optical densities are determined by these two parameters (i.e., group and phase velocity). We examine this question next using Maxwell's equations.

2.1 Maxwell's Equations

To study materials and their interaction with EM fields theoretically, a useful starting point is Maxwell's equations, which govern the dynamics of EM fields and charges. In Maxwell's equations, both μ and ε appear, as does the index of refraction, which describes the optical density of a material and appears as a combination of the two in the form $n = (\mu\varepsilon)^{1/2}$. In the usual treatments, we assume that the result is a positive number; however, it has been determined recently that this result (a positive number) is not the only possibility (see Eqs. (2.4)–(2.7)).

In the meter, kilogram, and second (mks) system of units and in a region without free charge, Maxwell's equations are as follows:

$$\nabla \cdot \varepsilon \boldsymbol{E} = 0, \tag{2.4}$$

$$\nabla \cdot \mu \boldsymbol{H} = 0, \tag{2.5}$$

$$\nabla \times \boldsymbol{E} = -\frac{\partial \mu \boldsymbol{H}}{\partial t}, \tag{2.6}$$

and

$$\nabla \times \boldsymbol{H} = \frac{\partial \varepsilon \boldsymbol{E}}{\partial t}, \tag{2.7}$$

where $\boldsymbol{E}$ is the electric field intensity in units of volts per meter and $\boldsymbol{H}$ is the magnetic field in units of amperes per meter. In these units, $\varepsilon = \varepsilon_0 = 8.85$ pF/m and the permeability is $\mu = \mu_0 = 1.25$ μHz/m. The equations could also be written using D, the electric flux density in units of coulomb per square meter, and B, the magnetic flux density, in units of Weber per square meter.

Assuming isotropic ε and μ, we can obtain the wave equation in the two forms:

$$\nabla^2 \boldsymbol{E} = \varepsilon\mu \frac{\partial^2 \boldsymbol{E}}{\partial t^2} \tag{2.8}$$

and

$$\nabla^2 \boldsymbol{H} = \varepsilon\mu \frac{\partial^2 \boldsymbol{H}}{\partial t^2}. \tag{2.9}$$

Clearly, $(\mu\varepsilon)^{-1/2}$ is the wave velocity in both forms. The flow of energy is given by $\boldsymbol{S} = \boldsymbol{E} \times \boldsymbol{H}$, where $\boldsymbol{S}$ is the Poynting's vector in units of Joules per meter^2-sec and the energy density is $u = (1/2)(\varepsilon \boldsymbol{E}^2 + \mu \boldsymbol{H}^2)$.

For demonstrating some basic phenomena, let us assume plane waves—specifically, a linear polarized beam with $\boldsymbol{E}$ in x direction ($\boldsymbol{H}$ in y direction), moving in the z direction with field sources

$$\mathrm{E} = E_0 \cdot \hat{x} \cdot e^{i(k \cdot z - \omega t)} \tag{2.10}$$

and

$$\mathrm{H} = \frac{kE_0}{\omega\mu} \cdot \hat{y} \cdot e^{i(k \cdot z - \omega t) + \frac{\pi}{2}}, \tag{2.11}$$

where $\boldsymbol{k} = k_z$ and $k^2 = \varepsilon\mu\omega^2$. The fields are perpendicular to each other and in a plane normal to the direction of propagation $\boldsymbol{k}$ as shown in Figure 1-1 in a vacuum. We have introduced a phase difference of $\pi/2$ between the E field (e.g., Eq. (2.10)) and the H field (e.g., Eq. (2.11)), realizing that although Eq. (2.8) and Eq. (2.9) are decoupled, the fields are actually related energy fields. The phase difference between the two fields makes the energy of the photon represented here constant during the whole cycle. The electric field feeds the magnetic field and vice versa.

Since we are only interested in real parts of $\boldsymbol{E}$ and $\boldsymbol{H}$, evaluating the time averaged Poynting vector $\boldsymbol{S}$ and the energy density U gives

$$\langle \boldsymbol{S} \rangle = \frac{1}{\omega\mu} \frac{E^2}{2} \cdot \boldsymbol{k} \tag{2.12}$$

and

$$\langle u \rangle = \frac{\langle \varepsilon \boldsymbol{E}^2 \rangle}{2} + \frac{\langle \mu \boldsymbol{H}^2 \rangle}{2} = \frac{1}{2}\left[\frac{1}{2}\varepsilon\, \boldsymbol{E}_0^2 + \frac{1}{2}\mu \boldsymbol{H}_0{}^2\right] = \frac{1}{2}\varepsilon\, \boldsymbol{E}^2 . \tag{2.13}$$

From Eq. (2.12), we see that when $\mu > 0$, $\boldsymbol{S}$ and $\boldsymbol{k}$ (energy and phase) are in the same direction), but, when $\mu < 0$, $\boldsymbol{S}$ and $\boldsymbol{k}$ (energy and phase) are in the opposite direction. This difference is a major distinction between normal materials and DNM and is the basis for later discussion.

Eq. 2-13 for the energy density applies to vacuum and PIR materials. For dispersive materials, the equation derived by Landau and Lifshitz[5] and used by Veselago[6] is

$$\langle u \rangle = \frac{\partial(\varepsilon\omega)}{\partial\omega}\, \boldsymbol{E}^2 + \frac{\partial(\mu\omega)}{\partial\omega}\, \boldsymbol{H}^2 . \tag{2.14}$$

For the energy density to be positive, the requirement on the derivatives is

$$\frac{\partial(\varepsilon\omega)}{\partial\omega} > 0, \frac{\partial(\mu\omega)}{\partial\omega} > 0 . \tag{2.15}$$

These requirements allow ε and μ to be simultaneously negative if they are functions of ω (i.e., $\varepsilon(\omega)$ and $\mu(\omega)$).

2.2 Possible Combinations of ε and μ in Materials

Now, if we consider Eq. (2.8) and Eq. (2.9) and look at all the possible combinations of ε and μ, we find that a propagating wave is supported by the material only when $\mu > 0$, $\varepsilon > 0$ and when $\mu < 0$, $\varepsilon < 0$. When $\mu > 0$, $\varepsilon < 0$ or when $\mu < 0$, $\varepsilon > 0$, the propagating wave decays and is not supported by the material, as shown in the μ–ε plot in Figure 2-1. Since no propagation can occur in these regions, they are not of interest here. When the product $\varepsilon\mu$ is positive, we get transmission across a boundary. When the product $\varepsilon\mu$ is negative, we get absorption at the boundary and no transmission through material.

---

5 Landau, L., and E. F. Lifshitz. *Electrodynamics of Continuous Media* (New York: Pergamon, 1960).

6 Veselago, V. G. January–February 1968. The electrodynamics of substances with simultaneously negative values of ε and μ. *Soviet Physics Uspekhi* 10 (4): 509–514. Available at http://www.iop.org/EJ/article/0038-5670/10/4/R04/PHU_10_4_R04.pdf?request-id=be94154d-cd29-4796-aca6-209e7c9b79bb

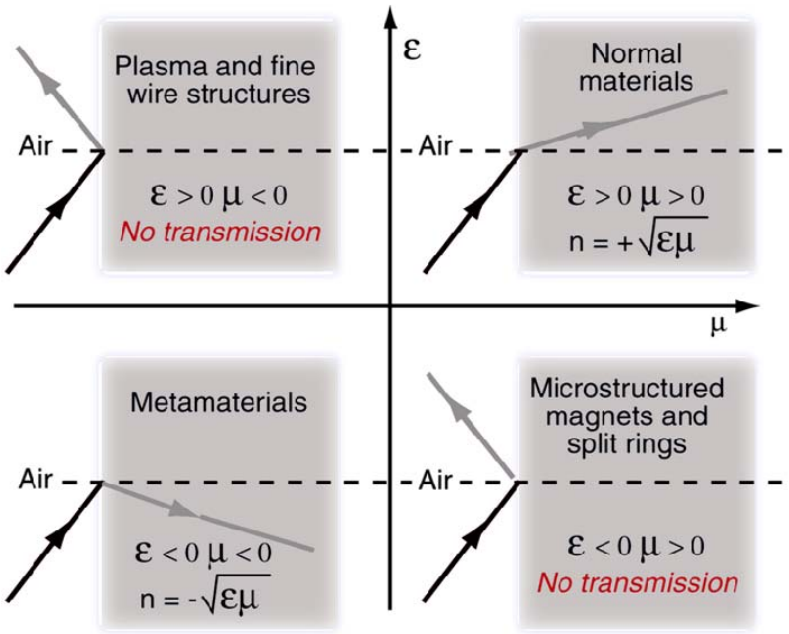

Figure 2-1. An EM Beam Interacting With Four Possible Materials

We now consider the conditions that lead to negative permittivity (ε) and negative permeability (μ) in materials. Negative values occur when resonances for the electric and the magnetic processes are in the materials. Negative refraction occurs when these resonances are at or near the same frequencies.

In most naturally occurring materials and over most frequencies, $\varepsilon > 0$ and $\mu > 0$. However, when resonances occur in a material, both $\varepsilon < 0$ and $\mu < 0$ can occur over a small range of frequencies. Generally, natural materials with $\varepsilon < 0$ occur over a region of the spectrum higher in frequency than those with $\mu < 0$. Thus, the frequency ranges are far apart, and they do not overlap, as shown in Figure 2-2. They are not expected to overlap in one material.

Negative ε occurs in metals in the optical region and in semiconductors in the terahertz to infrared (IR) region. Negative μ occurs at much lower frequencies, tailing off toward the terahertz and IR regions. Examples are as follows:

- ε negative in gold, silver, aluminum, and so forth
- μ negative in ferromagnetics or antiferromagnetics.

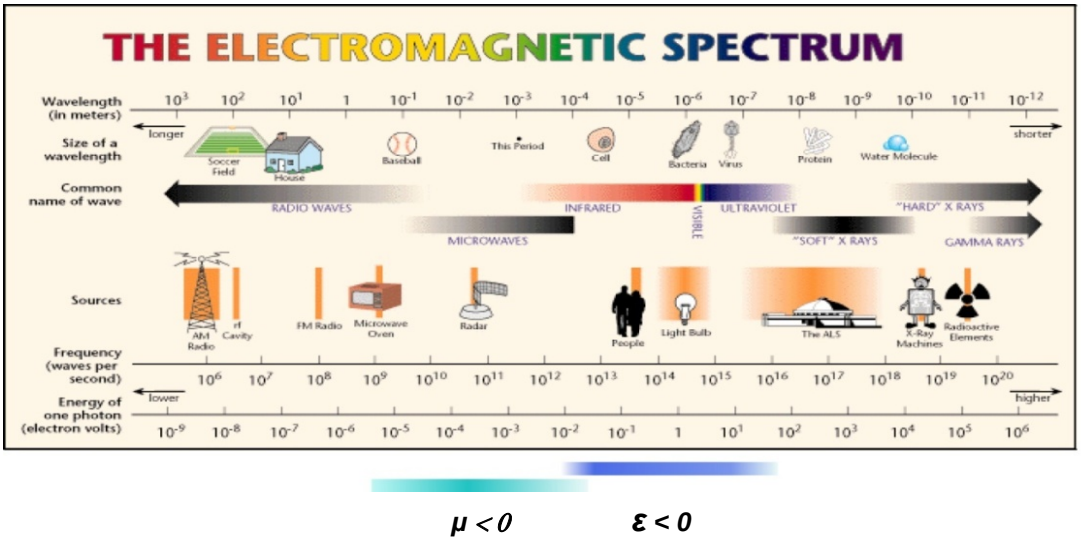

$\mu < 0$ $\varepsilon < 0$

Figure 2-3. EM Spectrum Showing Frequency Windows for Potential Location of Negative μ and ε in Natural Materials

Natural NIMs (ε and μ both negative) are rare, and early researchers thought they did not exist at all. However, some were reported recently. Pimenov et. al.[7] stated, "It is generally believed that nature does not provide materials with negative refraction . . ." but then the authors went on to describe just such a material: colossal magnetoresistance manganite ($La_{2/3}Ca_{1/3}MnO_3$) in a high magnetic field. The effect was demonstrated in 2007.

Another naturally occurring NIM is bismuth, which is active at a wavelength of $\lambda = 60$ μm.[8] One wonders how many others are to be discovered. These materials may have a high attenuation; therefore, they may not be useful for transmission. However, the index of refraction is still negative.

---

7 Pimenov, A., A. Loidl, K. Gehrke, V. Moshnyaga, and K. Samwer. "Negative Refraction Observed in a Metallic Ferromagnet in the Gigahertz Frequency Range." *Phys. Rev Lett.* 98 (19) (2007): 197401-1–197401-4.

8 Podolskiy, V. A., L. V. Alekseev, and E. E. Narimanov. "Strongly Anisotropic Media: The THz Perspectives of Left-Handed Materials." *Journal of Modern Optics* 52 (16) (2005): 2343–2349.

3. Basic Physics Phenomena

3.1 Radiating Dipole

In modeling the interaction of DNM, we are concerned with two processes:

1. How to model the absorption and emission of individual atoms, molecules, or other entities
2. How to model the transport of EM radiation through a real material.

The purpose of this modeling is not to provide answers to complex real situations but, instead, to show the phenomena in its simplest form. For the interaction of individual atoms with the radiation field, we will assume an electric dipole interacting with the EM field (see Figure 3-1) and model it as a forced harmonic oscillation with damping. The transport of radiation through a material will assume a change in velocity that results from a change in the density (i.e., index of refraction).

A radiating dipole produces the pattern of an equal plane of radiation, as shown in Figure 3-1. An EM field induces an absorption by the dipole. This absorption is followed by a reradiation of the EM energy. If the material is composed of atoms that have dipoles, the radiation is absorbed by the dipoles, which subsequently reradiate (elastic process) or absorb (inelastic process) and store the energy. These phenomena can be modeled as forced oscillations of a mass on a spring with drag.

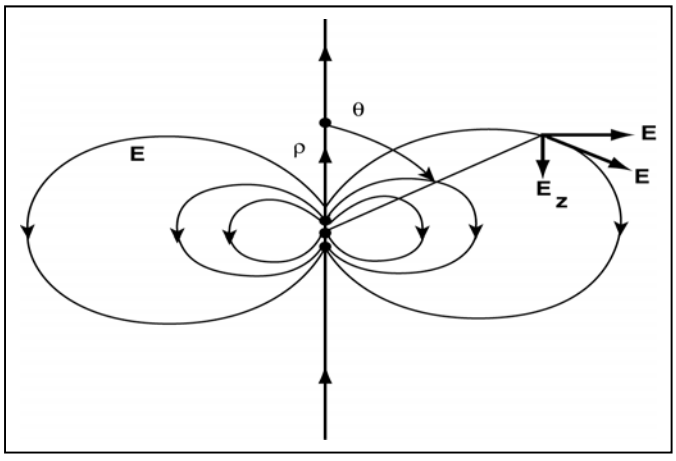

Figure 3-1. Electric Dipole Radiation Pattern

3.2. Resonances in Materials (Forced Oscillations – Mass on a Spring)

Resonance phenomena are exhibited by a simple model of a charge on a spring that is moving under the influence of an oscillating electric field. Figure 3-2 shows a small mass attached to an immovable wall. For our demonstration, this depiction models an electron attached to a much heavier atom under the influence of an oscillating force—an EM wave.

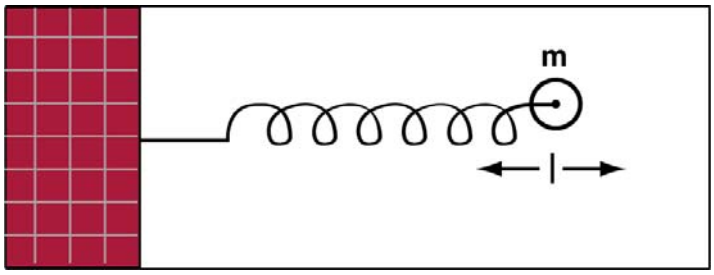

Figure 3-2. Mass on a Spring Attached to a Wall

Consider the motion of the small mass, *m*, influenced by an oscillating force $F\cos(\omega t)$ governed by

$$m\frac{d^2}{dt^2}X(t)+b\left(\frac{d}{dt}X(t)\right)+kX(t)=F_0\cos(\omega t), \tag{3.1}$$

where: $\omega_0=\sqrt{\frac{k}{m}}$, $\gamma=\frac{b}{2m}$, and $F_0=-eE$ represent the resonant frequency, the damping term, and the magnitude of the force, respectively.

The solution for the position is

$$X=\left(-\frac{eE}{m}\right)f(\omega,\omega_0)\cos(\omega t)+\left(-\frac{eE}{m}\right)g(\omega,\omega_0)\sin(\omega t), \tag{3.2}$$

where, $f(\omega,\omega_0)=\frac{(\omega_0{}^2-\omega^2)}{\left[(\omega_0{}^2-\omega^2)^2+4\gamma^2\omega^2\right]}$ and $g(\omega,\omega_0)=\frac{2\gamma\omega}{\left[(\omega_0{}^2-\omega^2)^2+4\gamma^2\omega^2\right]}$,

and, as we shall see, we can define the absorption amplitude as $A_{ab}=\left(-\frac{eE}{m}\right)g(\omega,\omega_0)$ and the elastic amplitude as $A_{el}=\left(-\frac{eE}{m}\right)f(\omega,\omega_0)$.

The amplitude of the elastic term $A_{el}=(-eE/m)f(\omega,\omega_0)$ and the absorptive term $A_{ab}=(-eE/m)g(\omega,\omega_0)$ is shown graphically in Figure 3-3. The constant A_{ab} is called the absorptive amplitude, and the constant A_{el} is called the elastic (or dispersive) amplitude

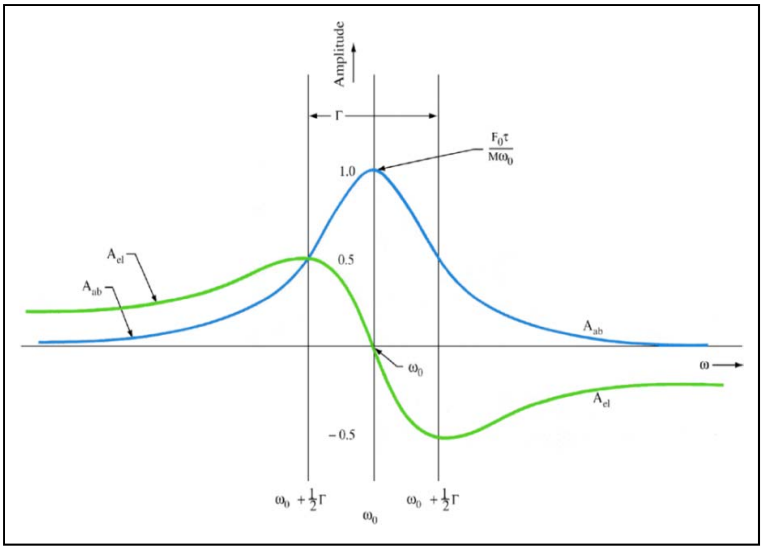

Figure 3-3. Absorptive (Blue) and Dispersive (Green) Amplitudes (Real and Imaginary Components in Some Developments Using Complex Notation) for the Response From a Forced Harmonic System

because of the way they deal with the input energy. The time-averaged input power absorption is entirely due to the $A_{ab}sin(\omega t)$ term. The $A_{el}cos(\omega t)$ term contributes to the instantaneous power absorption, $P(t)$, but averages to zero over one cycle of steady-state oscillation.

Therefore, since this energy is not absorbed, it must be transmitted or elastically scattered. These results follow from the fact that the instantaneous power, $P(t)$, is the force $F_0cos(\omega t)$ times the velocity $dx(t)/dt = (\omega A_{ab}cos(\omega t) - \omega A_{el}sin(\omega t))$. The instantaneous velocity has a contribution that is in phase with the force and a contribution that is 90 deg out of phase with the force. Only the velocity contribution that is in phase with the force contributes to the time-averaged power, P. This "in-phase velocity" is contributed by the "out-of-phase" displacement, $A_{ab}sin(\omega t)$.

This result is summarized as follows:

- Force:

$$F(t) = F_0 \cos(\omega t) \tag{3.3}$$

- Position-distance:

$$X(t) = A_{ab} \sin(\omega t) + A_{el} \cos(\omega t) \tag{3.4}$$

- Velocity:

$$\frac{dX}{dt} = -\omega A_{ab} \cos(\omega t) + \omega A_{el} \sin(\omega t) \tag{3.5}$$

- Instantaneous power absorbed (which is given by the product of force times velocity):

$$P(t) = F(t)(dX/dt) = F_0\omega A_{ab}(\cos(\omega t)\cos(\omega t)) - F_0\omega A_{el}(\cos(\omega t)\sin(\omega t)) \qquad (3.6)$$

- Average power over one cycle:

$$P = F_0\omega A_{ab} < \cos^2 \omega t > - F_0\omega A_{el} < \cos \omega t \sin \omega t > = \frac{1}{2} F_0\omega A_{ab} - 0\,. \qquad (3.7)$$

The medium is said to have normal dispersion when resonances are present in the material (e.g., at a frequency ω_0) and when to the left of the resonance ($\omega < \omega_0$), the index of refraction is increasing. The medium is said to have anomalous dispersion (which has been observed in atmospheric studies) when resonances are present in the material (e.g., at a frequency ω_0) and when to the right of the resonance ($\omega > \omega_0$), the index of refraction is decreasing. In some materials, the index of refraction could even become negative, which brings us to the topic of this study. We begin by looking first at resonance phenomena and then at the derivation of the index of refraction and its effect on EM waves transported through a medium composed of such resonances.

3.3 Calculation of the Index of Refraction: Transport Through a Plate

Let us assume a source at point S in vacuum that produces an oscillating EM field at point S given by

$$E_s = E_0\, e^{i\omega(t)}$$

and at point P is given by

$$E_s = E_0\, e^{i\omega(t - z/c)}\,. \qquad (3.8)$$

Inserting a plate of optically dense material of thickness Δz changes the field at P by slowing the velocity though the plate. The process of transport through the plate involves absorption and reemission of the EM field by resonances in the plate. One such event is pictured in the material in the plate shown Figure 3-4, but many events in the path of the beam contribute to the process.

As shown in Figure 3-4, the source, *S*, induces oscillation in the dipole in the material at point *z'*. Emissions from the oscillating dipole at point *z'* occur to the right and to the left from the dipole. However, we are only concerned with the emission to the right because this emission contributes to the field at point *P*, which changes from the

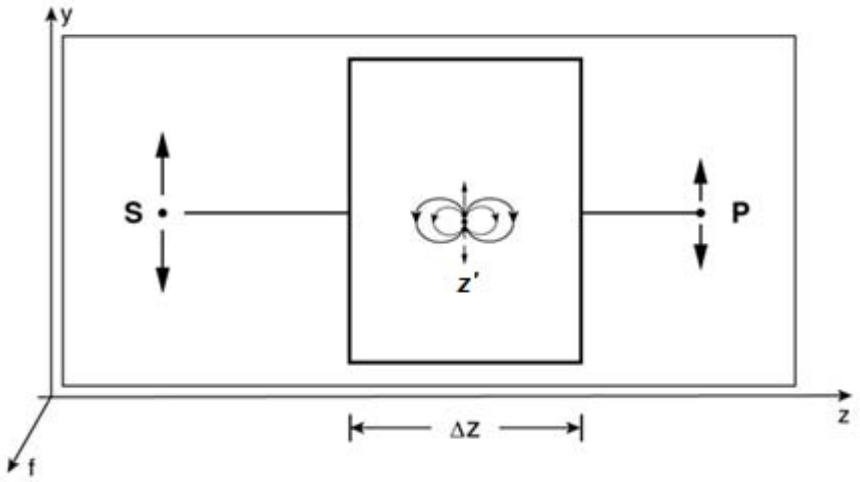

Figure 3-4. Transport of EM Radiation Through a Material Showing the Source (*S*), a Dipole Absorber/Emitter in the Material, and an External Point (*P*) at Which the Field Is Recorded

field in Eq. (3.8) to that shown in Eq. (3.9) because of the time delay Δt (Eq. (3.10)) caused by the dense plate of width Δz. The total field at point *P* is given by the sum of the source term (Eq. (3.8)) and the field produced by secondary sources in the plate:

$$E_p = E_0 e^{i\omega(t-\Delta t - z/c)}, \tag{3.9}$$

where

$$\Delta t = (n-1)\Delta z / c, \tag{3.10}$$

which comes from replacing the travel time through the region without the plate $\Delta z / c$ with the travel time through the plate and $n\Delta z / c$ lengthened by the index of refraction of the plate, *n*.

Expanding Eq. (3.9) using $e^{-x} \sim 1\text{-}x + \ldots$ etc. gives

$$E_p = E_0 e^{i\omega(t-z/c)} - i\omega(n-1)(\Delta z/c)E_0 e^{i\omega(t-z/c)}, \tag{3.11}$$

(source term) *(secondary sources in plate)*,

which is the source field and the field from the secondary source, clearly exhibited in Eq. (3.11).

We now go back to the analysis performed in Section 3.2 using real functions and reexpress with complex functions for which the analysis is more transparent. Again, the position of the charge is

$$X(t) = \frac{e \cdot E_0 \cdot e^{i\cdot\omega\cdot t}}{m(\omega_0^2 - \omega^2 + i\gamma\cdot\omega)}, \tag{3.12}$$

and the velocity of the charge is

$$\frac{dX(t)}{dt} = i \cdot \omega \cdot \frac{e \cdot E_0 \cdot e^{i \cdot \omega \cdot t}}{m(\omega_0^2 - \omega^2 + i\gamma \cdot \omega)}. \tag{3.13}$$

Using the result that a plane of oscillating charges with charge density η (charges per unit area), after integration over the plane produces a field at point z given by (see Feynman's Volume I)[9]

$$E_{TP}(t) = \frac{-\eta e}{2\varepsilon_0 c}[\text{velocity of charges at}(t - z/c)] \tag{3.14}$$

and inserting that field from Eqs. (3.12) and (3.13), we get

$$E_{TP}(t) = \frac{-\eta e}{2\varepsilon_0 c}(eE_0 / m) \cdot \frac{i \cdot \omega}{(\omega_0^2 - \omega^2 + i\gamma\omega)} \cdot e^{i\omega(t - z/c)}. \tag{3.15}$$

Now comparing Eq. (3.11) with Eq. (3.15) and realizing that they represent the same field, we get

$$(n-1)\Delta z = \frac{\eta e^2}{2\varepsilon_0 m(\omega_0^2 - \omega^2 + i\gamma\omega)}. \tag{3.16}$$

After solving for n, realizing that $N\Delta z = \eta$ and including the sum over possible different resonances k so that N_k is the volume density of k resonance, we get for the complex index of refraction

$$n = 1 + \frac{e^2}{2\varepsilon_0 m} \sum_k \frac{N_k}{\omega_k^2 - \omega^2 + i\gamma_k \omega}. \tag{3.17}$$

Sorting out the index into real and imaginary parts,

$$n = n' - in'', \tag{3.18}$$

we get an expression for the transmitted EM field that clearly reveals the absorption and elastic scattering parts:

$$E_s' = e^{-\omega n'' \Delta z / c} e^{-i\omega(n' - 1)\Delta z / c} E_0 e^{i\omega(t - z/c)} \tag{3.19}$$

[absorption] *[elastic scattering]*

---

9 Feynman, R. P., R. B. Leighton, and M. Sands. *Quantum physics.* Vol. 1 of *The Feynman Lectures on Physics* (Addison-Wesley, 1964).

The field at point P, after passing through the plate, is given by the product of a decaying exponential indicating absorption and a term representing the original source in front of the plate and the fields from secondary sources in the plate caused by elastic scattering. These solutions imply that negative values of *n* are possible in theory and are found at frequencies near resonances. Also, even though we have been talking about responses of atoms, we can replace the "atoms" in this system with man-made structures that give similar resonant effects, such as the split-ring resonator (SRR), nanowires, and so forth. Arrays of these structures will still have a total macroscopic effect of changing the velocity of EM radiation. These structures are examined in Section 5.

4. New Phenomena and Applications— or What Can We Do Now That We Could Not Do Before?

Department of Defense (DoD) technology developers and users are always looking for more effective and lighter components and devices for all conceivable applications. Metamaterials, or artificially engineered composite structures, have recently been receiving increasing attention. These novel artificial materials have numerous potential applications in science, technology, and medicine—especially if their novel behavior can be extended to the technologically critical near-IR and visible regions.

Engineers hope to exploit the extraordinary EM response that DNM offer. DNM exhibit a unique ability to bend and focus light in ways that no conventional materials can. The great potential for enabling several innovative structures will be explored in this section. To study the effect of these materials on EM propagation in various applications, we developed a computer model. Appendix D gives the theoretical basis for this model, and Appendix E shows some results obtained with the model.

The broad range commercial and DoD applications of these materials is contingent on extending the frequency range from microwaves to the optical region, broadening the frequency range of operability, and improving the understanding of the physics of their EM transport properties, all of which should lead to significant enhancements in the properties of these materials (bandwidth, loss, operational frequency, and so forth). However, we should mention that, at present, there are major limitations with many metamaterial designs. For example:

- Aspect angle dependence (not three-dimensional (3D))
- Polarization-dependent behavior
- Lossy
- Narrow band.

This section is divided into two parts

1. Phenomenology of the DNM or the new and unexpected physics
2. Interesting new things we can build with DNM.

Here, we discuss some applications that people thought of, others that people just dreamed about, and still others that were too strange to mention until now. Appendix F presents a more complete list of practical applications.

4.1 Reverse Cerenkov Radiation

An effect expected in double negative (DNG) materials is reversed Cerenkov radiation. Cerenkov radiation in normal materials is the result of charged particles traveling faster than the phase velocity of light in that material.

Figure 4-1 shows wave fronts (circles that represent points having the same phase) from moving charged particles when they travel slower than the speed of light in a normal material (a) and when they travel faster than the speed of light in the normal material (b) (circles represent points that have the same phase). The polarization of the molecules in the corresponding two cases is shown in Figure 4-2(a) and 4-2(b), where in normal media (a), the polarization is more symmetric around the charge and in (b) when the charge is moving faster than the speed of light in the medium, the polarization falls behind the charge.

Similar to the sonic boom observed at supersonic speeds, a coherent wave-front of light is emitted at a characteristic angle given by $cos(\theta) = 1/(\beta n)$, where $\beta = v/c$ and n is the index of refraction (see Figure 4-3).

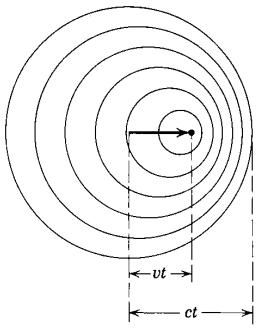

$v < c$

(a)

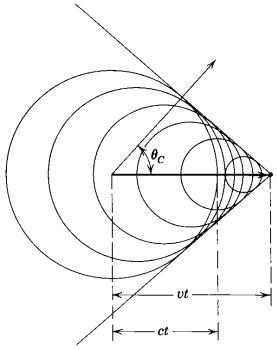

$v > c$

(b)

Figure 4-1. Wave Fronts for Charged Particles Moving (a) Slower and (b) Faster Than the Speed of Light in a Normal Material

If we consider a charged particle traveling in a DNG material, n is negative and the characteristic angle of the wave-front is obtuse. In other words, the Cerenkov

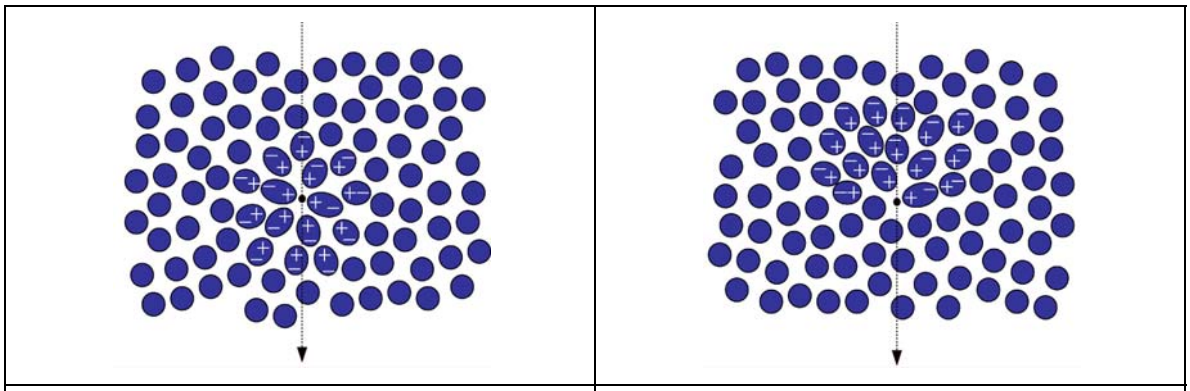

(a)	(b)

Figure 4-2. Polarization of Molecules in Normal Media for the Two Cases Shown in Figure 4-1(a) and 4-1(b)

Note for Figure 4-2: *Arrows show the velocity direction of the particle.*

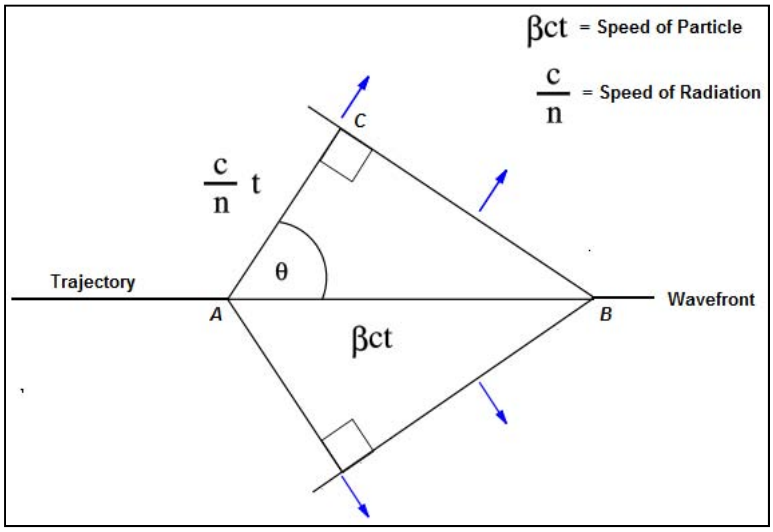

Figure 4-3. Geometry of Normal Cerenkov Radiation

radiation is emitted in the "backward" direction. Several analyses on Cerenkov radiation predict higher signals in DNG materials than in normal materials. Many speculate using this effect to create better Cerenkov detectors with DNG materials.

Figure 4-4 compares Cerenkov wave fronts in normal refraction materials (a) and DNM (b). In Figure 4-4(a), since the phase is traveling in the same direction as the energy, the wavelets from different positions combine so the wave front formed in the Cerenkov process is moving in the forward direction. In Figure 4-4 (b), the wavelets from different positions combine so the wave front is moving in the backward direction.

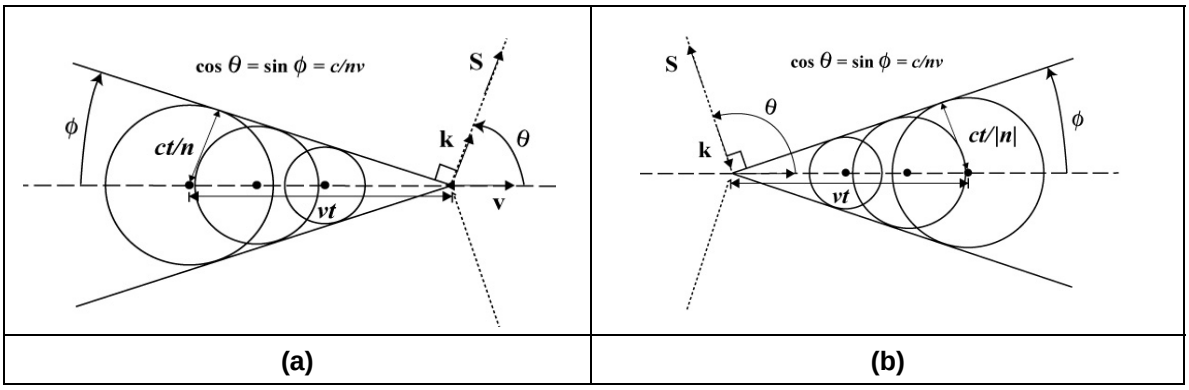

(a) (b)

Figure 4-4. (a) Normal Cerenkov Wave and (b) Reverse Cerenkov Wave Due To Transport Through a DNM

4.2 Reverse Doppler Effect

A remarkable consequence of negative phase velocities in DNG materials is a reverse Doppler effect (see Figure 4-5). In normal, right-handed media (a), the phase velocity is parallel to the group velocity. Therefore, when an observer approaches a radiating source, the observed frequency is higher than the emitted frequency. However, in left-handed media (b), the phase velocity is in the opposite direction. Therefore, instead of the "bunching" effect of wave fronts, an observer approaching a radiating source observes a lower frequency than the emitted frequency. This effect was predicted by Veselago and has been verified in several simulations and experiments involving left-handed transmission lines[10] and photonic crystals. However, the engineering of a reverse Doppler effect experiment in DNG materials still proves to be difficult.

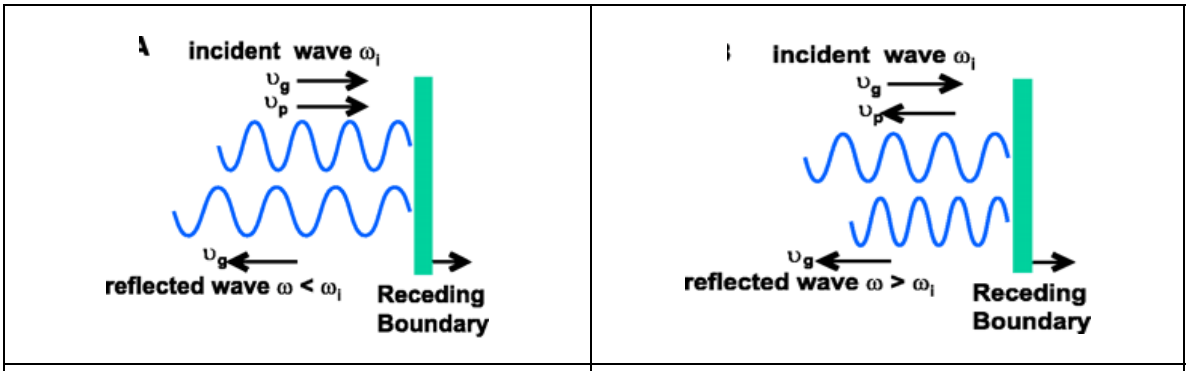

(a) (b)

Figure 4-5. Doppler Effect on Receding Boundary

10 Lai, Anthony, Christophe Caloz, and Tatsuo Itoh. "Composite Right/Left-Handed Transmission Line Metamaterials." *IEEE Microwave Magazine* 5 (3) (September 2004): 34–50.

4.3 Reverse Casimir Effect

The Casimir Effect is a force between two conductive surfaces in a vacuum caused by the difference in density of vacuum fluctuations[11] between the inside surfaces and outside the surfaces (see Figure 4-6). This difference reflects the fact that the frequency of fluctuations between the surfaces is limited to those virtual photons whose wavelengths fit a whole number of times into the gap. Thus, the effect is to bring the plates together so the force is attractive.

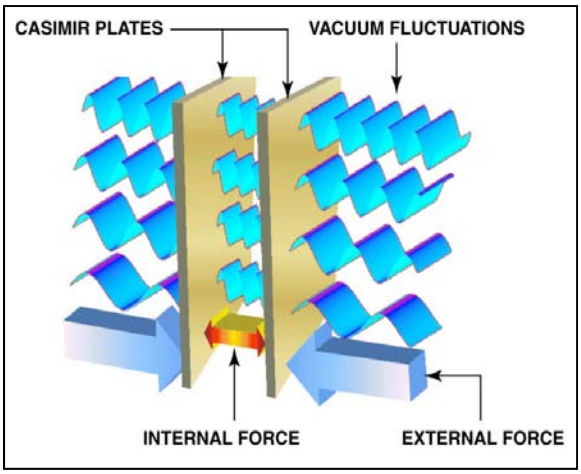

Figure 4-6. Difference in Vacuum Fluctuations Between Plates and an External Region for Normal Materials

The attractive Casimir force, $F_{Casimir}$, between two plates of area A separated by a distance L has been calculated:

$$F_{Casimir} = \frac{\pi \cdot h \cdot c}{480 \cdot L^4} A, \tag{4.1}$$

where h is Planck's constant and c is the speed of light.

We see from this equation that the plates have to be close together to get an appreciable effect. Assuming L = 1 μm and A = 1 m^2

$$F_{Casimir} = \frac{3.14 \cdot 6.6 \cdot 10^{-24} \cdot 3 \cdot 10^{8} \cdot 1}{480 \cdot 10^{-24}} = 1.3\, mN\,. \tag{4.2}$$

The gravitational force or weight of 1 kg is about 10 N, so 1.3 mN is the weight of 0.13 grams—small but measurable. Plates that have an area of 1 cm^2 at the same

---

11 A concept in quantum field theory where the virtual particles, photons, appear and disappear out of and into vacuum. Phenomena such as spontaneous emission, the Lamb Shift, and the Casimir Effect, can be explained in this way)

separation would feel a force equivalent to the weight of about 10^{-5} grams or a force of approximately 10^{-7}N. This force is quite small but is now within the range of modern laboratory force measurement techniques. This force has been measured by various research groups, and even detailed measurements investigating the effect as a function of the thickness and material properties of the plates have been accomplished.[12]

On the other hand, inserting a DNM between the plates produces a reverse effect, and the force becomes repulsive, as suggested by several theoretical investigations.[13],[14] The negative-index metamaterial (according to researchers) is able to modify the zero-point fluctuations between the surfaces by focusing the photons and reversing the direction of the Casimir force. This repulsive force is strong enough (according to researchers) to levitate an aluminum mirror 500-nm thick, causing it to hover above a perfect lens placed over a conducting plate. At the present time, we do not have any experimental verification of this reverse effect. Much controversy and much interest have been generated in the community. This concept is theoretical—no experimental observations yet.

This reverse Casimir effect could be very important in the fabrication and application of small systems because, as small as it is, the normal Casimir effect contributes to viscosity in nanosystems and causes parts in nanosystems and Microelectromechanical Systems (MEMS) to stick together. The reverse effect could be used to alleviate the problems.

4.4 Reverse Snell's Law

In a normal transparent (dielectric) material, an EM beam is refracted to the right as shown in Figure 1-2. The angle of refraction is obtained from Snell's law, which states that the ratio of the sines of the angles of incidence and refraction is equal to the ratio of velocities in the two media or, equivalently, to the inverse ratio of the indices of refraction n_1 and n_2. Thus,

$$n_1 \sin(\theta_1) = n_2 \sin(\theta_2), \tag{4.3}$$

---

12 Capasso, F., J. N. Munday, D. Iannuzzi, and H. B. Chan. "Casimir Forces and Quantum Electrodynamical Torques: Physics and Nanomechanics." *Selected Topics in Quantum Electr., IEEE Journal of* 13 (2) (2007): 400–414.

13 Leonhardt, U., and T. G. Philbin. "Quantum Levitation by Left-Handed Metamaterials." *New J. Phys.* 9 (254) (2007): 1–11.

14 Kenneth, O., I. Klich, A. Mann, and M Revzen. "Repulsive Casimir Forces." *Phys. Rev. Lett.* 89 (3) (15 July 2002): 033001-1–033001-4.

where θ_1 and θ_2 are the angles of incidence and refraction, respectively.

In a DNM, the law still holds, but, since $n_2 < 0$, and $\theta_2 < 0$, $n_2 sin(\theta_2)$ is still positive, the beam direction is to the left, as shown in Figure 1-2.

4.5 Metamaterials as a Perfect Lens

Probably the most talked about and controversial application of DNM the ability to focus incident waves from a source beyond the diffraction limit. In other words, DNM can be used to create perfect lenses, with no theoretical limit on resolution.

The idea of a perfect lens was first proposed by Pendry.[15] To summarize Pendry's argument, consider a radiating source in a vacuum and a lens with an axis parallel to the z-axis. For a given emitted frequency, ω, the emitted radiation will have the following Fourier composition:

$$\sum_{\sigma,k_x^2,k_y^2} E\sigma(k_x,k_y)\exp(i(k_x x + k_y y + k_z z - \omega t)), \tag{4.4}$$

where $\boldsymbol{k} = k_x \boldsymbol{x} + k_y \boldsymbol{y} + k_z \boldsymbol{z}$, $\boldsymbol{z}$ is the wave vector of the Fourier component, and σ denotes the polarization. The wave vector components and the frequency, ω, satisfy the free-space (positive refractive index) dispersion relation. This constrains the value of k_z:

$$k_z = \sqrt{\omega^2 c^2 - k_x^2 - k_y^2}\,. \tag{4.5}$$

According to Eq. (4.5), the maximum real value for k_z is $|\boldsymbol{k}| = \omega c$, where c is the speed of light in the medium. However, Maxwell's equations allow for solutions where $k_x^2 + k_y^2 > (\omega c)^2$. In these cases, k_z is positive imaginary and it is possible for $|k_z| > |\boldsymbol{k}|$. These modes of emission are known as evanescent waves. From Eq. (4.4), positive imaginary k_z implies the amplitude of evanescent modes decay exponentially. Therefore, to examine modes of emission for $|k_z| > |\boldsymbol{k}|$ (i.e., subwavelength modes), the lens needs to be very close (i.e., subwavelength distances) to the source. Also, for normal lenses, these modes will still decay in the lens once transmitted. Thus, evanescent modes are essentially ignored and the theoretical limit on the wavelength of radiation that can be focused by a normal lens is determined by $k_{max} = |\boldsymbol{k}|$:

---

15 deWolf, D. A. "Transmission of Evanescent Wave Modes Through a Slab of DNG Material." *IEEE Transactions on Antennas and Propagation* 53 (1) (January 2005): 270274. Available at http://ieeexplore.ieee.org/stamp/stamp.jsp?arnumber=01377601

$$\Delta \approx \frac{2\pi}{k_{\max}} = \frac{2\pi c}{\omega} = \lambda \,. \tag{4.6}$$

Now suppose the lens is a DNM metamaterial that is negatively matched to vacuum (i.e., $\varepsilon_r = \mu_r = -1$). According to Pendry, the information from the evanescent waves can, in theory, be recovered with such a lens. As discussed in previous sections, DNM are left-handed systems, where the dispersion relation gives a phase velocity (or the wave vector) that is anti-parallel to the group velocity. Therefore, if the group velocity does not change at the interface of the lens, the wave vector inside the lens is the negative of the wave vector in vacuum, (i.e., $\boldsymbol{k}' = -\boldsymbol{k}$). This sign reversal also applies to evanescent modes. With $k_z' = -k_z$, the evanescent modes exponentially grow instead of decay inside the lens, which implies that a DNM can amplify evanescent modes, and, therefore, subwavelength information can be recovered from the source, as shown in Figure 4-7.

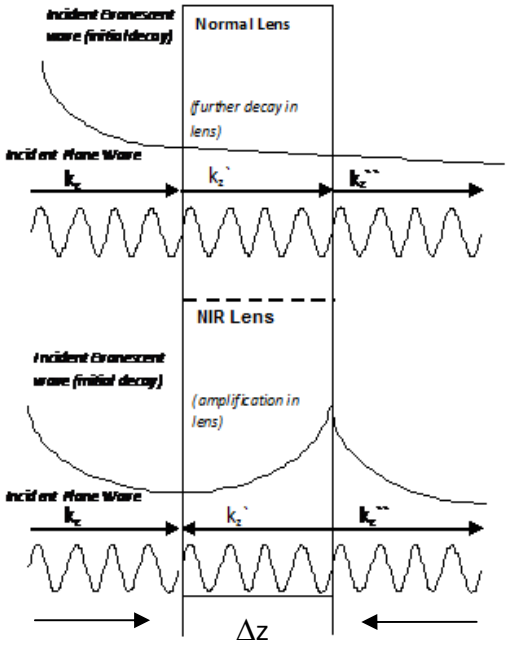

Figure 4-7. Simple Illustration of Perfect Lensing

Note for Figure 4-7: *The top half represents a normal lens where evanescent waves continue to decay. The bottom half represents a DNM lens, where evanescent waves are amplified.*

The amplification of the evanescent wave in the DNM (as shown in Figure 4-7) has been discussed in the literature by people who argue that this amplification leads to unphysical results. However, it also has been defended on the basis (1) that natural attenuation in real materials presents the divergences in ideal situations from occurring or

(2) that when the time development of the wave in the material is examined, divergences are suppressed.[16]

According to Pendry's argument, a perfect lens with arbitrarily small resolution can be constructed with DNM, and applications of such perfect lenses would be vast. However, several academics are skeptical of these claims. The most noted critics in the literature are P. Valanju at University of Texas-Austin and N. Garcia and M. Nieto-Vesperinas of Spain's Higher Council for Scientific Research in Madrid. Valanju challenges not only Pendry, but also Veselago's original paper on negative refraction. Valanju argues that negative refraction violates causality and requires information to travel faster than the speed of light. Garcia and Nieto-Vesperinas, however, are in agreement with Veselago's results but argue that a perfect lens would require infinite energy density.

Many experiments have been motivated by this debate, and several authors have reported observing perfect lens effects in DNM for small frequency intervals. An example of such an observation was reported by Lagarkov and Kissel,[17],[18] who report being able to image separately two radiating radio sources that are separated by less than a wavelength using a DNM.

Despite the supporting experimental results, many are still skeptical of the idea of a perfect lens. This skepticism is mainly due to the many hurdles physicists and engineers must overcome to construct a practical working perfect lens. Currently, the main limitation in all reported perfect lenses is the limited frequency range of effect. Also, an ideal, perfect lens would have isotropic DNM properties, which many researchers are finding difficult to construct. Attenuation of signals is also a problem with current DNM.

---

16 Gómez-santos, G. "Universal Features of the Time Evolution of Evanescent Modes in a Left-Handed Perfect Lens." *Phys. Rev. Lett.* 90 (7) (21 February 2003): 077401-1–077401-4. Available at http://prola.aps.org/pdf/PRL/v90/i7/e077401

17 Lagarkov, A. N., and V. N. Kissel. "Near-Perfect Imaging in a Focusing System Based on a Left-Handed-Material Plate." *Phys. Rev. Lett.* 92 (7) (2004): 077401-1–077401-4.

18 Kissell, V. N., and A. N. Lagarkov. "Superresolution in Left-Handed Composite Structures: From Homogenization to a Detailed Electrodynamic Description." *Phys. Rev. B.* 72 (8) (2005): 085111-1–085111-8.

4.6 Cloaking/Invisibility

A potential application of metamaterials that has recently gained a great deal of attention is the ability to create EM cloaking materials. According to Pendry et al.,[19] if given a metamaterial with flexible EM properties (i.e., control over the permittivity and permeability tensors), light can be forced to wrap around an enclosed space without scattering (see Figure 4-8). In other words, the enclosed space is rendered invisible. Several simulations have supported Pendry's claim, and Schurig et al.[20] have achieved two-dimensional (2D) cloaking in the microwave regime for a copper cylinder.

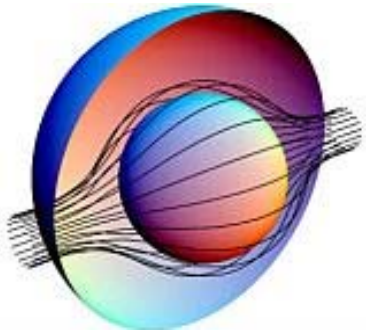

Figure 4-8. An Artist's Rendition of EM Waves Traveling Around an Enclosed Space

Metamaterials that would serve such a purpose are not necessarily DNG materials, but anisotropic media with very complex material properties. Fabrication of such complex metamaterials would take advantage of the many experimental advances made in fabricating DNG materials, so these subjects are related. The emerging field of tailoring ε and μ to suit an application like cloaking is called "transformation optics."

---

19 Pendry, J. B., D. Schurig, and D. R Smith. "Controlling Electromagnetic Fields." *Science* 312 (7) (June 2006): 1780–1782.

20 Schurig, D., J. J. Mock, B. J. Justice, S. A. Cummer, J. B. Pendry, A. F. Starr, and D. R. Smith. "Metamaterial Electromagnetic Cloak at Microwave Frequencies." *Science* 314 (5801) (10 November 2006): 977–980.

5. Manufacturing an NIM

To construct DNM or NIR materials, we need to have electric and magnetic resonances occur at the same frequency. Pendry et al., suggested the use of SRRs for the magnetic response[21] and short wire antennas for the electric response.[22] A structure of thin wires, as shown in Figure 5-1, supports plasmons with a plasma frequency dependent only on the geometry of the structure and given by

$$\omega_p = 2 \cdot \pi \cdot c^2 / (a^2 \ln(a/r)), \tag{5.1}$$

where *r* is the wire radius. The Drude permittivity is given by

$$\varepsilon(\omega) = \varepsilon_0 (1 - \omega_p^2 / \omega^2). \tag{5.2}$$

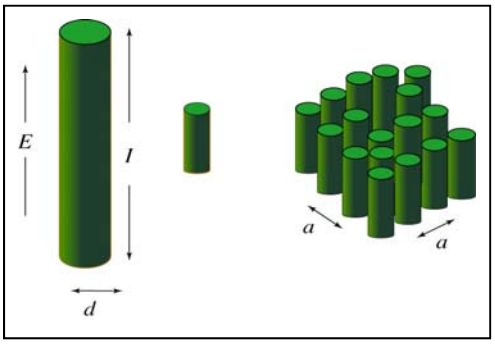

Figure 5-1. Wire Structure

For the magnetic response refer to the structure shown in Figures 5-2 and 5-3 and eq. 5.3. The frequency-dependent permeability, $\mu(\omega)$, for this structure is given by

$$\mu(\omega) = 1 - \frac{\frac{\pi r^2}{a^2}}{1 + \frac{2l\sigma_1}{\omega r \mu_0} i - \frac{3lc^2}{\pi\omega^2 \ln\left(\frac{2b}{d}\right) r^3}}. \tag{5.3}$$

---

21 Pendry, J. B., A. J. Holden, D. J. Robbins, and W. J. Stewart. "Magnetism From Conductors and Enhanced Nonlinear Phenomena." *IEEE Trans. Microwave Theory Tech.* 47 (11) (1999): 2075–2081.

22 Pendry, J. B., A. J. Holden, W. J. Stewart, and I. I. Youngs. "Extremely Low-Frequency Plasmons in Metallic Mesostructures. *Phys. Rev. Lett.* 76 (25) (1996): 4773–4776.

The parameters *a*, *l*, *b*, *d*, and *r* are defined in Figures 5-2–5-4, *c* is the speed of light in a vacuum, and σ_1 is the resistance of unit length measures around the circumference of the rings. The resonant frequency, ω_0, for this structure is given by

$$\omega_0^2 = \frac{3lc^2}{\pi \ln\left(\frac{2b}{d}\right) r^3}. \tag{5.4}$$

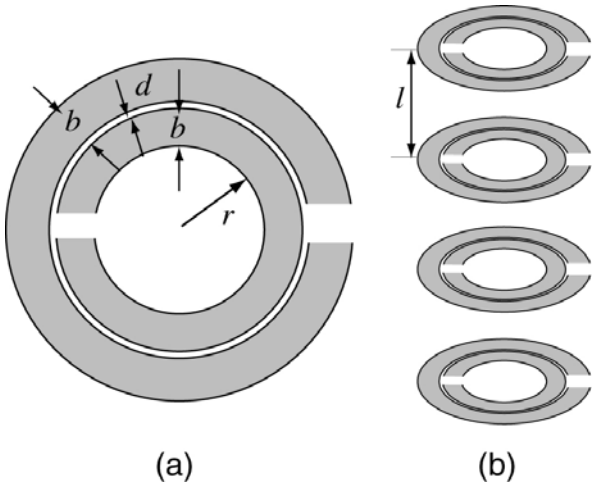

Figure 5-2. (a) Plan View of a Split Ring Showing Definitions of Distances; (b) Sequence of Split Rings Shown in Their Tracking Sequence

Source: Adapted from Pendry, J. B., A. J. Holden, D. J. Robbins, and W. J. Stewart. 1999. Magnetism from conductors and enhanced nonlinear phenomena. *IEEE Trans. Microwave Theory Tech.* 47:2075–2084.

Note for Figure 5-2: *Each split ring comprises two thin sheets of metal.*

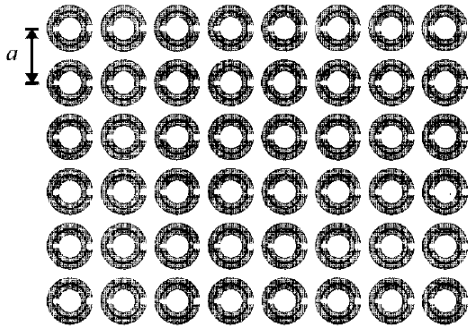

Figure 5-3. Plan View of a Split-Ring Structure in a Square Array (Lattice Spacing "*a*")

Source: Pendry, J. B., A. J. Holden, D. J. Robbins, and W. J. Stewart. 1999. Magnetism from conductors and enhanced nonlinear phenomena. *IEEE Trans. Microwave Theory Tech.* 47:2075–2084.

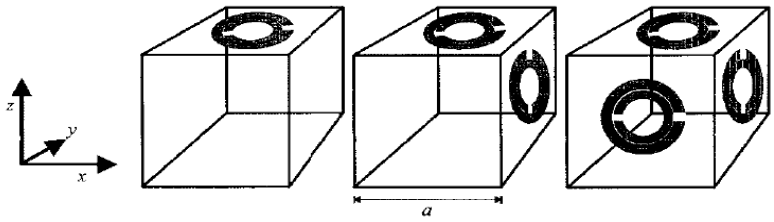

Figure 5-4. Constructing an Isotropic Material

Source: Pendry, J. B., A. J. Holden, D. J. Robbins, and W. J. Stewart. 1999. Magnetism from conductors and enhanced nonlinear phenomena. *IEEE Trans. Microwave Theory Tech.* 47:2075–2084.

Note for Figure 5-4: *An isotropic material is constructed by repeating the unit cell on the right in three dimensions.*

Following Pendry's suggestion, SRRs and wire antennas were used in early attempts to produce DNM in the megahertz region. Figure 5-5 shows one of the early models of a DNM (metamaterial) used for the megahertz regime. Figure 5-6 shows the Boeing cube, another early structure used for the gigahertz regime. As Eq. (5.1) and Eq. (5.4) show, the resonant frequency for these structures increases as their size decreases. To build materials that exhibit negative refraction at the higher frequencies, researchers eventually miniaturized these structures to tens of nanometers in size. However, manufacturing double SRRs at this scale became too difficult and costly. As a result, single split rings became more common. Other methods that permitted smaller sizes and higher frequencies were also used. Eventually, researchers turned to single split rings and wires in the nano regime, as shown in Figure 5-7.

Figure 5-5. Wire and Split-Ring Structure Designed for the Megahertz Range

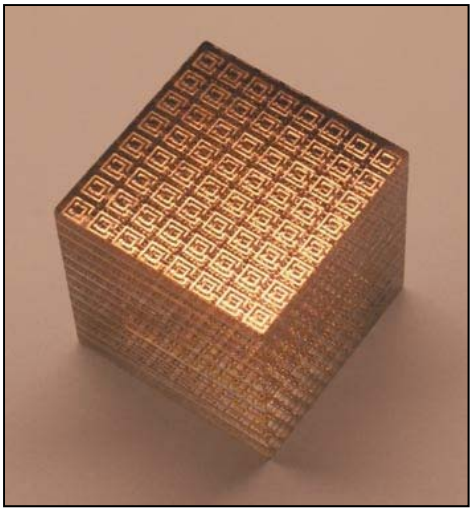

Figure 5-6. Boeing Cube Structure Designed for the Gigahertz Range

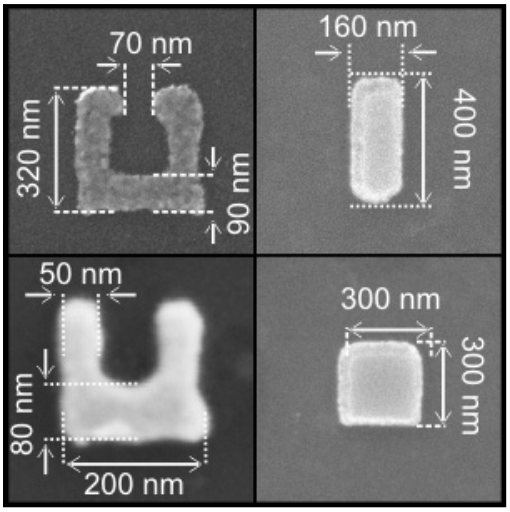

Figure 5-7. Wire and Split-Ring Structures for Higher Frequencies

Eventually nanorings and nanoantennas reached their limit of usefulness because the small sizes resulted in lower conductivity. Even silver, with its high electrical conductivity, ran into problems at this scale. This point is noteworthy because even though SRRs and nanowire antennas obtain their μ and ε characteristics from their geometric structures (see Eqs. (5.1)–(5.3)), high conductivity and low dissipation are implicitly required for their utility.

To reach even higher frequencies, other approaches, such as the fishnet structure shown in Figure 5-8, became favored. All these changing structures are a trend to get into the optical regime.

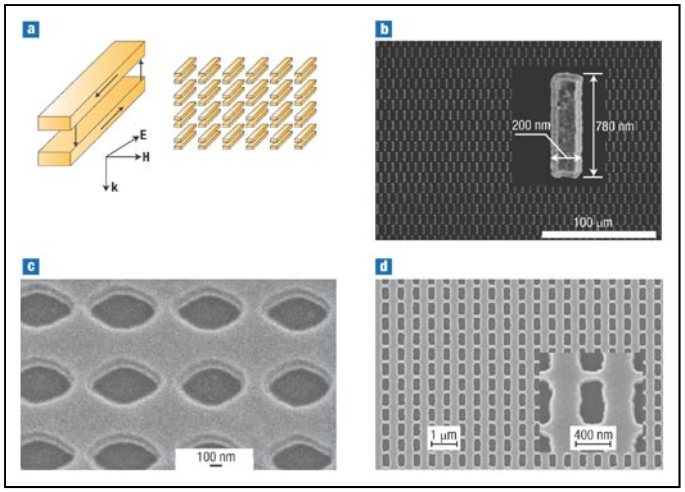

Figure 5-8. Fishnet Structures for Higher Frequencies

Figure 5-9 shows the trends in the development of DNM to reach the optical regime and their experimental realizations. Instead of split rings and wires, fishnet designs with dielectric plates between conductors, as shown in Figure 5-8 and to the right in Figure 5-9, became popular in 2006. The most recent theoretical suggestion is to get away from rings and wires and fishnet designs and use (1) plasmon resonant metal nano-particles,[23],[24] (2) nanofabricated photonic materials,[25] or (3) dielectric nanoparticles coated with conductive layers.[26],[27] These densely packed particle designs are expected to provide not only DNM properties in the optical regime but also produce 3D behavior.

---

23 Klar, T. A., Kildishev, A. V., Drachev, V. P., and Shalaev, V. M. "Negative Index Materials: Going Optical." *Selected Topics in Quantum Electronics, IEEE Journal of* 12 (6) (November–December 2006): 1106–1115.

24 Valentine, Jason, Shuang Zhang, Thomas Zentgraf, Erik Ulin-Avila, Dentcho A. Genov, Guy Bartal, and Xiang Zhang. "Three Dimensional Optical Metamaterial With a Negative Refractive Index." *Nature* 455 (18 September 2008): 376–379.

25 Lezec, H. J, Dionne, J. A., Atwater, H. A. "Negative Refraction at Visible Frequencies." *Science* 316 (5823) (20 April 2007): 430–432.

26 Yannopapas, V. "Artificial Magnetism and Negative Refractive Index in Three-Dimensional Metamterials of Spherical Particles at Near-Infrared and Visible Frequencies." *Appl. Phys. A* 87 (2) (2007): 259–264.

27 Alù, A., and N. Engheta. "Polarizabilities and Effective Parameters for Collections of Spherical Nanoparticles Formed by Pairs Of Concentric Double-Negative (DNG), Single-Negative (SNG) and/or Double-Positive (DPS) Metamaterial Layers." *J. Appl. Phys* 97 (9) (May 2005): 094310-1–094310-12.

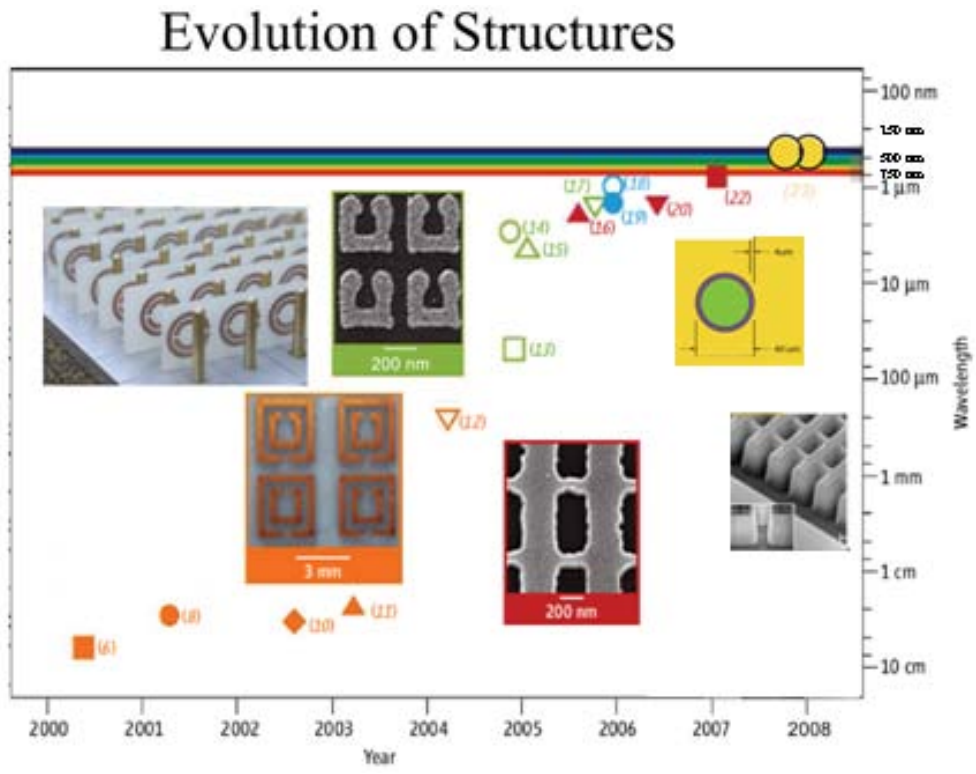

Figure 5-9. Trends in the Development of Metamaterials From Split Rings to Wire-Mesh Fishnet to Dielectric Nanoparticles

Source: Adapted from Soukoulis, C. M., S. Linden, and M. Wegener. January 2007. "Negative refractive index at optical wavelengths negative refractive index at optical wavelengths." *Science* 315 (5808): 47–49.

Note for Figure 5-9. *The solid symbols denote $n < 0$, the open symbols denote $\mu < 0$. Insets show fabricated structures in different frequency regimes. Color scheme: double SRRs (orange), U-shaped SRR (green), metallic nanorods (blue), fishnet structures (red), nanospheres (yellow coated).*

Glossary

2D	two-dimensional
3D	three-dimensional
ABC	Absorbing Boundary Condition
AMC	Artificial Magnetic Conductor
APMC	Asia-Pacific Microwave Conference
CD	compact disk
CRP	Central Research Program
DARPA	Defense Advanced Research Projects Agency
DNG	double-negative
DNM	double negative material
DPS	double-positive
DSO	Defense Sciences Office
EM	electromagnetic
FDTD	finite-difference time-domain
FY	Fiscal Year
IDA	Institute for Defense Analyses
IEEE	Institute of Electrical and Electronics Engineers, Inc.
IR	infrared
IWON	International Workshop on Nanoscience and Nanotechnology
LHM	left-handed material
MELECON	Mediterranean Electrotechnical Conference
MEMS	microelectromechanical systems
NFSL	near-field superlens
NGV	negative group velocity
NIM	negative index material
NIR	negative index of refraction
NLO	non-linear optics
PIER	Progress In Electromagnetics Research
PIR	positive index of refraction
RHM	right-handed material
RRL	Rapid Research Letters
SHG	second-harmonic generation
SNG	single-negative
SSR	split-ring resonator

Appendix A.
October 2008 Briefing: Double Negative Materials (DNMs)

This appendix is on a compact disk (CD) attached to the inside back cover of this document. The briefing on DNMs was presented in October 2008. It contains movie clips (pages A-7, A-29, and A-30) that show a simulation of EM waves propagating through normal material and through DNM.

Double Negative Materials (DNMs)

Bohdan Balko
John Franklin
John Biddle

October2008

Appendix B.
Glossary for Double Negative Materials (DNMs)

Abbe limit (diffraction limit): A limitation of conventional optics. The resolution (i.e., level of detail) that such optical systems can achieve is limited by diffraction to approximately half the wavelength of the light being used.

Babinet's principle: A law of diffraction stating that the diffraction pattern generated by an opaque object is the same as that generated by a hole of the same size and shape, except for the intensity of the pattern.

Cerenkov effect: An effect that arises when a charged particle, such as an electron, moves through a medium at a speed faster than the speed of light in that medium. (Relativity dictates only that a particle must travel with a speed less than or equal to that of light in a vacuum, whereas in a non-vacuum, light may be slowed down more than the particle. When a particle moves through a medium with faster-than-light speed, it emits radiation known as Cerenkov radiation.) The direction of this radiation is different in negative-index materials vs. positive-index materials.

Doppler effect: A change in the frequency of a wave due to relative motion between the source and the observer of the wave.

Far field: The region whose distance from a source of radiation is many times the wavelength of that radiation.

Left-handed material: Conventional materials, which have a positive index of refraction, obey a physical principle known as the "right-hand rule." Thus, these conventional materials are called "right-handed." In contrast, negative-index materials are called "left-handed."

Metamaterial: A material whose microscopic or nanoscopic structure is designed to produce unusual behaviors at a macroscopic level. For example, a negative-index metamaterial can be constructed using electromagnetic (EM) resonators that are much smaller than the wavelength of light for which negative index is desired. At the size scale of the light waves, the resonators are "invisible" (i.e., only the bulk behavior of the material can be seen).

Near field: The region close to a source of radiation, typically within one wavelength of the source.

Near-field superlens (NFSL): A general superlens could be constructed from a material that has negative refractive index (i.e., negative electric permittivity and negative magnetic permeability). A special case is the NFSL. The principle underlying the NFSL is that in the near field, negative

permittivity alone is sufficient to achieve the superlensing effect. Thus, an NFSL could be constructed from a negative-permittivity film (e.g., silver). This type of superlens requires that the film be sufficiently thin and that the object is sufficiently close to the lens.

Negative-index material: A material that has a negative index of refraction (i.e., that simultaneously has negative electric permittivity and negative magnetic permeability).

Non-linear optics (NLO): Optics that employs media with nonlinear permittivity (i.e., where the permittivity, ε, varies with the intensity of the light and, thus, the strength of the electric field). Examples of NLO include second-harmonic generation and optical parametric amplification.

Optical parametric amplification: A mechanism for generating a laser light with a tunable wavelength.

Perfect lens: A lens that can resolve images below the Abbe limit (see preceding definition). Such a lens can be constructed using a negative-index material.

Phase: A measure of the distance from a given reference point to the nearest peak of a wave.

Phase anisotropy: A situation where light waves with different polarizations have different phases (see also “Phase” and “Polarization”).

Phase shift: A difference in phase between two waves of the same frequency. Equivalently, a spatial or temporal offset between these waves.

Polarization: A light wave is composed of oscillating electric and magnetic fields. Polarization refers to the directions in which these fields point.

Second-harmonic generation (SHG): A nonlinear optical process in which two photons interact with a nonlinear material to combine and produce a single photon of twice the frequency.

Superlens: See “Perfect lens.”

Appendix C.
Bibliography for Double Negative Materials (DNMs)

Alu, A., A. Salandrino, and N. Engheta. "Negative Effective Permeability and Left-Handed Materials at Optical Frequencies." *Opt. Express* 14, no. 4 (February 20, 2006): 1557–567. Available at http://www.opticsinfobase.org/DirectPDFAccess/8A3F7158-BDB9-137E-CB10E147158DA675_88069.pdf?da=1&id=88069&seq=0&CFID=45143136&CFTOKEN=48950826

Alu, A., and N. Engheta. "Polarizabilities and Effective Parameters for Collections of Spherical Nanoparticles Formed by Pairs of Concentric Double-Negative (DNG), Single-Negative (SNG), and/or Double-Positive (DPS) Metamaterial Layers." *J. Appl. Phys.* 97, no. 9 (May 2005): 094310-1–094310-12.

Alu, A., and N. Engheta. "Three-Dimensional Nanotransmission Lines at Optical Frequencies: A Recipe for Broadband Negative-Refraction Optical Metamaterials." *Phys. Rev. B* 75, no. 2 (2007): 024304-1–024304-20.

Bai, Y., H. Chen, J. Zhang, Y. Luo, B. Li, L. Ran, J. A. Kong, and J. Zhou. "Left-Handed Material Based on Ferroelectric Medium." *Opt. Express* 15, no. 13 (June 25, 2007): 8284–8289. Available at http://www.opticsinfobase.org/DirectPDFAccess/8A3E7786-BDB9-137E-C3C153FB9C4DABB6_138576.pdf?da=1&id=138576&seq=0&CFID=45143136&CFTOKEN=48950826

Bayindir, M., K. Aydin, E. Ozbay, P. Markos, and C. M. Soukoulis. "Transmission Properties of Composite Metamaterials in Free Space." *Appl. Phys. Lett.* 81, no. 1 (2002): 120–122.

Bulu, I., H. Caglayan, and E. Ozbay. "Experimental Demonstration of Labyrinth-Based Left-Handed Metamaterials." *Opt. Express* 13, no. 25 (December 12, 2005): 10238–10247. Available at http://www.opticsinfobase.org/DirectPDFAccess/8A3D89AB-BDB9-137E-C9ED72EAEA7FE3AC_86466.pdf?da=1&id=86466&seq=0&CFID=45143136&CFTOKEN=48950826

Caloz, C., A. Lai, and T. Itoh. "Wave Interactions in a Left-Handed Mushroom Structure." In *Antennas and Propagation Society International Symposium (IEEE)*, Vol. 2 (20–25 June 2004): 1403–1406. Available at http://www.ee.ucla.edu/~antlai/files/Lai_APS_2004.pdf

Caloz, C., F. P. Casares-Miranda. "Active Metamaterial Structures and Antennas." Paper presented at *IEEE MELECON 2006*, May 16–19, Malaga, Spain. Available at http://ieeexplore.ieee.org/ielx5/11001/34649/01653090.pdf?isnumber=34649

Chettiar, U. K., A. V. Kildishev, H-K. Yuan, W. Cai, S. Xiao, V. P. Drachev, and V. M. Shalaev. "Double Negative Index Metamaterial: Simultaneous Negative Permeability and Permittivity at 812 nm." In *Photonic Metamaterials: From Random to Periodic*, OSA Technical Digest (CD) (Optical Society of America, 2007): Conference paper MA3. Available at http://www.opticsinfobase.org/DirectPDFAccess/D6CA5B99-BDB9-137E-C18F1F7A8AC4E1FE_138818.pdf?da=1&id=138818&seq=0&CFID=25309117&CFTOKEN=82080576

Chettiar, U. K., A. V. Kildishev, T. A. Klar, and V. M. Shalaev. "Negative Index Metamaterial Combining Magnetic Resonators With Metal Films." *Opt. Express* 14, no. 7 (August 21, 2006): 7872–7877. Available at http://www.opticsinfobase.org/DirectPDFAccess/8A3C5438-BDB9-137E-C832F6AAB7141200_97675.pdf?da=1&id=97675&seq=0&CFID=45143136&CFTOKEN=48950826

Dolling, G., C. Enkrich, M. Wegener, C. M. Soukoulis, and S. Linden. "Simultaneous Negative Phase and Group Velocity of Light in a Metamaterial." *Science* 312, no. 5775 (12 May 2006): 892–894.

Dolling, G., C. Enkrich, M. Wegener, J. F. Zhou, C. M. Soukoulis, and S. Linden. "Cut-Wire Pairs and Plate Pairs as Magnetic Atoms for Optical Metamaterials." *Optics Letters* 30, no. 23 (2005): 3198–3200. Available at http://www.opticsinfobase.org/DirectPDFAccess/8A3B4DC4-BDB9-137E-C6A88162D23C971F_86374.pdf?da=1&id=86374&seq=0&CFID=45143136&CFTOKEN=48950826

Dolling, G., M. Wegener, C. M. Soukoulis, and S. Linden. "Negative-Index Metamaterial at 780 nm Wavelength." *Opt. Lett.* 32, no. 1 (2007): 53–55.

Fan, X., G. Wang, J. C. W. Lee, and C. T. Chan. "All-Angle Broadband Negative Refraction of Metal Waveguide Arrays in the Visible Range: Theoretical Analysis and Numerical Demonstration." *Phy. Rev. Lett.* 97, no. 7 (2006): 073901-1–073901-4.

Foteinopoulou, S. M. Kafesaki, E. N. Economou, and C. M. Soukoulis. "Backward Surface Waves at Photonic Crystals." *Phys. Rev. B* 75, no. 24 (2007): 245116-1–245116-6.

Gao, X., W. Xu, and F. Gan. "The Tunable Negative Refractive Index in Granular Composite." *Phys. Lett. A* 339, nos. 1–2 (2005):123–130.

Grbic, A. "A 2-D Composite Medium Exhibiting Broadband Negative Permittivity and Permeability." In *Antennas and Propagation Society International Symposium 2006, IEEE* (9–14 July 2006): 4133–4136. Available at http://ieeexplore.ieee.org/ielx5/11208/36089/01711538.pdf?isnumber=36089

Grigorenko, A. N., A. K. Geim, H. F. Gleeson, Y. Zhang, A. A. Firsov, I. Y. Khrushchev, and J. Petrovic. "Nanofabricated Media With Negative Permeability at Visible Frequencies." *Nature* 438, no. 7066 (17 November 2005): 335–338.

He, Y., P. He, S. D. Yoon, P. V. Parimi, F. J. Rachford, V. G. Harris, and C. Vittoria. "Tunable Negative Index Metamaterial Using Yttrium Iron Garnet." *Journal of Magnetism and Magnetic Materials* 313, no. 1 (June 2007): 187–191. Available at http://www.cm3ic.neu.edu/pubs/YHe_JMMM2007.pdf

Hudlicka M., J. Machae, and S. Nefedov. "A Triple Wire Medium as an Isotropic Negative Permittivity Metamaterial." *Progress In Electromagnetics Research (PIER)* 65 (2006): 233–246. Available at http://ceta.mit.edu/pier/pier65/16.06102703.Hudlicka.MN.pdf

Ishikawa, A., T. Tanaka, and S. Kawata. "Negative Magnetic Permeability in the Visible Light Region." *Phys. Rev. Lett.* 95, no. 23 (2005): 237401-1–237401-4.

Jiang, J., J. Cai, G. P. Nordin, and L. Li. "Parallel Microgenetic Algorithm Design for Photonic Crystal and Waveguide Structures." *Opt. Lett.* 28, no. 23 (2003): 2381–2383. Available at http://www.opticsinfobase.org/DirectPDFAccess/8A37F2D0-BDB9-137E-CBBDCBD8576FF9AB_78025.pdf?da=1&id=78025&seq=0&CFID=45143136&CFTOKEN=48950826

Kastel, J., M. Fleischhauer, S. F. Yelin, and R. L. Walsworth. "Tunable Negative Refraction Without Absorption via Electromagnetically Induced Chirality." *Phys. Rev. Lett.* 99, no. 7 (2007): 073602-1–073602-4.

Kildishev, A. V., U. K. Chettiar, Z. Liu, V. M. Shalaev, D.-H. Kwon, Z. Bayraktar, and D. H. Werner. "Stochastic Optimization of Low-Loss Optical Negative-Index Metamaterial." *J. Opt. Soc. Am. B* 24, no. 10 (October 2007): A-34–A-39.

Klein, M. W., C. Enkrich, M. Wegener, C. M. Soukoulis, and S. Linden. "Single-Slit Split-Ring Resonators at Optical Frequencies: Limits of Size Scaling." *Opt. Lett.* 31, no. 9 (May 1, 2006): 1259–1261. Available at http://www.opticsinfobase.org/DirectPDFAccess/8A364ABD-BDB9-137E-C9CB806022B85E21_89265.pdf?da=1&id=89265&seq=0&CFID=45143136&CFTOKEN=48950826

Kong, J. A., T. M. Grzegorczyk, Z. M. Thomas, H. Chen, and L. Ran. "Application of Hyperbolic Dispersion Relations of Left-Handed Metamaterials." In the *Microwave Conference Proceedings, 2005. APMC 2005. Asia-Pacific Conference Proceedings*, Vol. 1 (4–7 December 2005): 4 pp. Available at http://ieeexplore.ieee.org/stamp/stamp.jsp?arnumber=01606178

Lezec, H., J. A. Dionne, and H. A. Atwater. "Negative Refraction at Visible Frequencies." *Science* 316, no. 5823 (20 April 2007): 430–432.

Linden, S., C. Enkrich, G. Dolling, M. W. Klein, J. Zhou, T. Koschny, C. M. Soukoulis, S. Burger, F. Schmidt, and M. Wegener. "Photonic Metamaterials: Magnetism at Optical Frequencies." *IEEE Journal of Selected Topics in Quantum Electronics* 12, no. 6 (2006): 1097–1105.

Linden, S., C. Enkrick, M. Wegener, J. Zhou, T. Koschny, and C. M. Soukoulis. "Magnetic Response of Metamaterials at 100 Terahertz." *Science* 306, no. 5700 (19 November 2004): 1351–1353.

Liu, Y., N. Fang, D. Wu, C. Sun, and X. Zhang. "Symmetric and Antisymmetric Modes of Electromagnetic Resonators." *Appl. Phys. A* 87, no. 2 (2007): 171–174.

Liu, Z., U. K. Chettiar, A. V. Kildishev, V. M. Shalaev, D-.H. Kwon, Z. Bayraktar, and D. H. Werner. "Optical Negative Index Metamaterials With Low Losses: Nature-Inspired Methods for Optimal Design." In *Photonic Metamaterials: From Random to Periodic*, OSA Technical Digest (CD) (Optical Society of America, 2007): Conference paper TuB23. Available at http://www.opticsinfobase.org/DirectPDFAccess/D6CFE605-BDB9-137E-C3B3ECEFAA88A64E_138866.pdf?da=1&id=138866&seq=0&CFID=25309117&CFTOKEN=82080576

Mackay, T. G., and A. Lakhtakia. "Negative Phase Velocity in a Uniformly Moving, Homogeneous, Isotropic, Dielectric-Magnetic Medium." *J. Phys. A: Math. Gen.* 37, no. 21 (2004): 5697–5711.

Maksimović, M., and Z. Jakšić. "Emittance and Absorptance Tailoring by Negative Refractive Index Metamaterial-Based Cantor Multilayers." *J. Opt. A: Pure Appl. Opt.* 8, no. 3 (2006): 355–362.

Maksimović, M., and Z. Jakšić. "Fibonacci-Type Quasi-Periodic Nanocomposite Filters Containing Negative Index Metamaterials for Emittance Tailoring." In *Proc. 1st International Workshop on Nanoscience & Nanotechnology (IWON) 2005*, Belgrade, Serbia (2005): 190–193. Available at http://nanosys.ihtm.bg.ac.rs/staff/Jaksic_publications/Radovi/Maksimovic%202005%20-%20Fibonacci%20NRM%20-%20IWON.pdf

Marques, R., F. Mesa, J. Martel, and F. Medina. "Comparative Analysis of Edge- and Broadside-Coupled Split Ring Resonators for Metamaterial Design – Theory and Experiments." *IEEE Transactions on Antennas and Propagation* 51, no. 10 (October 2003): 2572–2581.

Marques, R., L. Jelinek, and F. Mesa. "Negative Refraction From Balanced Quasi-Planar Chiral Inclusions." *Microwave and Optical Technology Letters* 49, no. 10 (2007): 2606–2609. Available at http://www3.interscience.wiley.com/cgi-bin/fulltext/114297963/PDFSTART

McCall, M. W. "Classical Gravity Does Not Refract Negatively." *Phys. Rev. Lett.* 98, no. 9 (2007): 091102-1–091102-4.

Oliveira, S. L., and S. C. Rand. "Intense Nonlinear Magnetic Dipole Radiation at Optical Frequencies: Molecular Scattering in a Dielectric Liquid." *Phys. Rev. Lett.* 98, no. 9 (2007): 093901-1–093901-4.

Ozbay, E., I. Bulu, and H. Caglayan. "Transmission, Refraction, and Focusing Properties of Labyrinth Based Left-Handed Metamaterials." *Phys. Stat. Sol. B* 244, no. 4 (2007): 1202–1210.

Padilla, W. J., M. T. Aronsson, C. Highstrete, M. Lee, A. J. Taylor, and R. D. Averitt. "Novel Electrically Resonant Terahertz Metamaterials." arXiv:cond-mat/0605002v1 (2006). Available at http://arxiv.org/abs/cond-mat/0605002

Pendry, J. B., A. J. Holden, D. J. Robbins, and W. J. Stewart. "Magnetism From Conductors and Enhanced Nonlinear Phenomena." *IEEE Transactions on Microwave Theory and* Techniques 47, no. 11 (November 1999): 2075–2084.

Pinchuk, A. O., and G. C. Schatz. "Metamaterials With Gradient Negative Index of Refraction." *J. Opt. Soc. Am. A* 24, no. 10 (2007): A-39–A-44. Available at http://www.opticsinfobase.org/DirectPDFAccess/8A4366FD-BDB9-137E-CD587E36AF2F55F7_141204.pdf?da=1&id=141204&seq=0&CFID=45143136&CFTOKEN=48950826

Popov, A. K., S. A. Myslivets, T. F. George, and V. M. Shalaev. "Tailoring Transparency of Negative-Index Metamaterials With Parametric Amplification." Paper presented at *Metamaterials 2007: First International Congress in Advanced Electromagnetic Materials in Microwaves and Optics*, Rome, Italy (22–26 October 2007). Available at http://cobweb.ecn.purdue.edu/~shalaev/MURI/publications/PMGSh_META_Rome_Tailoring_NIM_Transparency.pdf

Popov, A. K., S. A. Myslivets, T. F. George, and V. M. Shalaev. "Compensating Losses in Positive- and Negative-Index Metamaterials Through Nonlinear-Optical Quantum Switching." In *Conference on Lasers and Electro-Optics/Pacific Rim 2007*, (Optical Society of America) (2007): Conference paper MG1_2. Available at http://www.opticsinfobase.org/DirectPDFAccess/D6D349FA-BDB9-137E-CE486599D1228FE7_157663.pdf?da=1&id=157663&seq=0&CFID=25309117&CFTOKEN=82080576

Ren, K., Z. Y. Li, X. Ren, B. Cheng, and D. Zhang. "Tunable Negative Refraction by Electro-Optical Control in Two-Dimensional Photonic Crystal." *Appl. Phys. A* 87, no. 2 (2007): 181–185.

Rochholz, H., N. Bocchio, and M. Kreiter. "Tuning Resonances on Crescent-Shaped Noble-Metal Nanoparticles." *New J. Phys.* 9, no. 3 (2007): 53-1–53-18. Available at http://www.iop.org/EJ/article/1367-2630/9/3/053/njp7_3_053.pdf?request-id=34df9cea-2377-406b-9031-cd1074b9e6c3

Rockstuhl, C, and F. Lederer. "Negative-Index Metamaterials From Nanoapertures." *Phys. Rev. B* 76, no. 12 (2007): 125426-1–125426-6.

Rockstuhl, C., and F. Lederer. "Design of an Artificial Three-Dimensional Composite Metamaterial With Magnetic Resonances in the Visible Range of the Electromagnetic Spectrum." *Phys. Rev. Lett.* 99, no. 1 (2007): 017401-1–017401-4.

Schurig, D., J. J. Mock, and D. R. Smith. "Electric-Field-Coupled Resonators for Negative Permittivity Metamaterials." *Appl. Phys. Lett.* 88, no. 4 (2006): 041109-1–041109-3.

Shen, J. T., P. B. Catrysse, and S. Fan. "Mechanism for Designing Metallic Metamaterials With a High Index of Refraction." *Phys. Rev. Lett.* 94, no. 19 (2005): 197401-1–197401-4.

Simovski, C. R., and S. He. "Frequency Range and Explicit Expressions for Negative Permittivity and Permeability for an Isotropic Medium Formed by a Lattice of Perfectly Conducting Ω Particles." *Phys. Lett. A* 311, nos. 2–3 (12 May 2003): 254–263.

Starr, A. F., P. M. Rye, D. R. Smith, and S. Nemat-Nasser. "Fabrication and Characterization of Negative-Refractive-Index Composite Metamaterial." *Phys. Rev. B* 70, no. 11 (2004): 113102-1–113102-4.

Tretyakov, S. A. "Meta-Materials With Wideband Negative Permittivity and Permeability." *Microwave and Optical Technology Letters* 31, no. 3 (2001): 163–165. Available at http://www3.interscience.wiley.com/cgi-bin/fulltext/85511266/PDFSTART

Voskoboynikov, O., G. Dyankov, C. M. J. Wijers. "Left Handed Composite Materials in the Optical Range." *Microelectronics Journal* 36, nos. 3–6 (2005): 564–566. Available at http://www.sciencedirect.com/science?_ob=MImg&_imagekey=B6V44-4FNP2RY-4-W&_cdi=5748&_user=1825799&_orig=search&_coverDate=06%2F30%2F2005&_sk=999639996&view=c&wchp=dGLbVlW-zSkWA&md5=6a6200061c0fc9da6148efa36772e910&ie=/sdarticle.pdf

Wang, F. M., H. Liu, T. Li, Z. G. Dong, S. N. Zhu, and X. Zhang. "Metamaterial of Rod Pairs Standing on Gold Plate and Its Negative Refraction Property in the Far-Infrared Frequency Regime." *Phys. Rev. E* 75, no. 1 (2007): 016604-1–016604-4.

Wang, F.-M., H. Liu, T. Li, S.-N. Shu, and X. Zhang. "Omnidirectional Negative Refraction With Wide Bandwidth Introduced by Magnetic Coupling in a Tri-Rod Structure." *Phys. Rev. B* 76, no. 7 (2007): 075110-1–075110-4.

Wang, X., D.-H. Kwon, D. H. Werner, I.-C. Khoo, A. V. Kildishev, V. M. Shalaev. "Tunable Optical Negative-Index Metamaterials Employing Anisotropic Liquid Crystals." *Appl. Phys. Lett.* 91, no. 14 (2007): 143122-1–143122-3.

Wang. Y.-Y., and L.-W. Chen. "Tunable Negative Refraction Photonic Crystals Achieved by Liquid Crystals." *Opt. Express* 14, no. 22 (October 30, 2006): 10580–10587. Available at http://www.opticsinfobase.org/DirectPDFAccess/8A34A9AE-BDB9-137E-C06C37E26EEE671E_116572.pdf?da=1&id=116572&seq=0&CFID=45143136&CFTOKEN=48950826

Werner, D. H., D.-H. Kwon, I.-C. Khoo, A. V. Kildishev, and V. M. Shalaev. "Liquid Crystal Clad Near-Infrared Metamaterials With Tunable Negative-Zero-Positive Refractive Indices." *Opt. Express* 15, no. 6 (March 19, 2007): 3342–3347. Available at http://cobweb.ecn.purdue.edu/~shalaev/Publication_list_files/liquid_crystal.pdf

Wheeler, M. S., J. S. Aitchinson, and M. Mojahedi. "Three-Dimensional Array of Dielectric Spheres With an Isotropic Negative Permeability at Infrared Frequencies." *Phys. Rev. B* 72, no. 19 (2005): 193103-1–193103-4.

Wongkasem, N., A. Akyurtlu, and K. A. Marx. "Group Theory Based Design of Isotropic Negative Refractive Index Metamaterials." *Progress In Electromagnetics Research (PIER)* 63 (2006): 295–310. Available at http://ceta.mit.edu/PIER/pier63/17.06062103.Wongkasem.AM.pdf

Wongkasem, N., A. Akyurtlu, J. Li, A. Tibolt, Z. Kang, and W. D. Goodhue. "Novel Broadband Terahertz Negative Refractive Index Metamaterials: Analysis and Experiment." *Progress in Electromagnetics Research (PIER)* 64 (2006): 205–218. Available at http://ceta.mit.edu/PIER/pier64/13.06071104.Wongkasem.ALTKG.pdf

Yannopapas, V. "Artificial Magnetism and Negative Refractive Index in Three-Dimensional Metamaterials of Spherical Particles at Near-Infrared and Visible Frequencies." *Appl. Phys. A* 87, no. 2 (2007): 259–264.

Yannopapas, V. "Negative Refraction in Random Photonic Alloys of Polaritonic and Plasmonic Microspheres." *Phys. Rev. B* 75, no. 3 (2007): 035112-1–035112-7.

Yannopapas, V. "Negative Refractive Index in the Near-UV From Au-Coated CuCl Nanoparticle Superlattices." *Phys. Stat. Sol. (RRL)* 1, no. 5 (2007): 208–210.

Yao, H.-Y., L.-W. Li, Q. Wu, and J. A. Kong. "Macroscopic Performance Analysis of Metamaterials Synthesized From Microscopic 2-D Isotropic Cross Split-Ring Resonator Array." *Progress In Electromagnetics Research (PIER)* 51 (2005): 197–217. Available at http://ceta.mit.edu/PIER/pier51/12.0402031.Y.Li.WK.pdf

Yen, T. J., W. J. Padilla, N. Fang, D. C. Vier, D. R. Smith, J. B. Pendry, D. N. Basov, and X. Zhang. "Terahertz Magnetic Response From Artificial Materials." *Science* 303, no. 5663 (5 March 2004): 1494–1496.

Yuan, H.-K., W. Cai, U. K. Chettiar, V. D. Silva, A. V. Kildishev, A. Boltasseva, V. P. Drachev, and V. M. Shalaev. "Metamagnetics for Visible Wavelengths (491–754 nm)." In *Photonic Metamaterials: From Random to Periodic*, OSA Technical Digest (CD) (Optical Society of America, 2007): Conference paper MA4. Available at http://www.opticsinfobase.org/DirectPDFAccess/D6D55519-BDB9-137E-C626453BFB38DFC3_138819.pdf?da=1&id=138819&seq=0&CFID=25309117&CFTOKEN=82080576

Zhang, H., Y. Niu, and S. Gong. "Electromagnetically Induced Negative Refractive Index in a V-Type Four-Level Atomic System." *Phys. Lett. A* 363, nos. 5–6 (2007): 497–501.

Zhang, S., W. Fan, B. K. Minhas, A. Frauenglass, K. J. Malloy, and S. R. J. Brueck. "Midinfrared Resonant Magnetic Nanostructures Exhibiting a Negative Permeability." *Phys. Rev. Lett.* 94, no. 3 (2005): 037402-1–037402-4.

Zhang, S., W. Fan, K. J. Malloy, S. R. J. Brueck, N. C. Panoiu, and R. M. Osgood. "Near-Infrared Double Negative Metamaterials." *Opt. Express* 13, no. 13 (June 27, 2005): 4922–4930. Available at http://www.chtm.unm.edu/publications/OE_sz.pdf

Zhang. S., W. Fan, N. C. Panoiu, K. J. Malloy, R. M. Osgood, and S. R. J. Brueck. "Experimental Demonstration of Near-Infrared Negative-Index Metamaterials." *Phys. Rev. Lett.* 95, no. 13 (2005): 137404-1–137404-4.

Zhou, J., T. Koschny, L. Zhang, G. Tuttle, and C. M. Soukoulis. "Experimental Demonstration of Negative Index of Refraction. *Appl. Phys. Lett.* 88, no. 22 (2006): 221103-1–221103-3.

Zhou, X., Q. H. Fu, J. Zhao, Y. Yang, and X. P. Zhao. “Negative Permeability and Sub-wavelength Focusing of Quasi-Periodic Cell Metamaterials.” *Opt. Express* 14, no. 16 (August 7, 2006): 7188–7197. Available at http://www.opticsinfobase.org/DirectPDFAccess/8A301791-BDB9-137E-CCFB5D8AA89D584C_96199.pdf?da=1&id=96199&seq=0&CFID=45143136&CFTOKEN=48950826

Ziolkowski, R. W., and C.-Y Cheng. “Existence and Design of Trans-Vacuum-Speed Metamaterials.” *Phys. Rev. E* 68, no. 2 (2003): 026612-1–026612-18.

Appendix D.
Computer Model of Electromagnetic (EM) Propagation in Double Negative Materials (DNMs)

D.1 Computer Model

In our algorithm, we use the material model introduced in 1900 by Paul Drude. Other investigators use variations on modeling this phenomena, but, for this study, we feel the "lossy Drude model" is sufficient. Drude assumed that the interaction of a material with EM waves was well modeled by a charge on a spring attached to a wall or a much heavier mass, subject to a damping force and to an oscillating force. Resonances arising from this interaction produce the interesting phenomena that we want to investigate. With these assumptions, the permeability and permittivity are

$$\varepsilon(\omega) = \varepsilon_0\left(1 - \frac{\omega_{pe}^2}{\omega(\omega + i\Gamma_e)}\right) \quad \omega_{pe}, \omega_{pm} \text{ "electric/magnetic plasma frequency"} \quad \text{(D.1)}$$

and

$$\mu(\omega) = \mu_0\left(1 - \frac{\omega_{pm}^2}{\omega(\omega + i\Gamma_m)}\right) \quad \Gamma_e, \Gamma_m \text{ "electric/magnetic collision frequency."} \quad \text{(D.2)}$$

The frequency domain equations[1] for the complex permittivity and permeability permit a frequency domain description of electric and magnetic current density:

$$\mathbf{P}(\omega) = i\omega\varepsilon_0 \frac{\omega_{pe}^2}{i\omega\Gamma_e - \omega^2}\mathbf{E}(\omega) \quad \text{(D.3)}$$

and

$$\mathbf{M}(\omega) = i\omega\mu_0 \frac{\omega_{pm}^2}{i\omega\Gamma_m - \omega^2}\mathbf{H}(\omega). \quad \text{(D.4)}$$

---

1 Jackson, J. D. *Classical Electrodynamics*. 3rd ed. (New York: John Wiley and Sons, 1998).

One obtains the time-domain versions of these equations by first rearranging the equations like and then exploiting algebraic properties of the Fourier transform. Given $x(t)$ and $X(\omega)$ where $X(\omega)=\frac{1}{\sqrt{2\pi}}\int_{-\infty}^{\infty}x(t)\exp(-i\omega t)dt$, we derive the Fourier transform, $X'(\omega)$, of $\partial_t x(t)$ in terms of $X(\omega)$:

$$\begin{aligned}
X'(\omega) &= \lim_{\varepsilon\to 0}\frac{1}{\varepsilon}\left[-X(\omega)+\frac{1}{\sqrt{2\pi}}\int_{-\infty}^{\infty}x(u)\exp(-i\omega u+i\omega\varepsilon)du\right] \\
&= \lim_{\varepsilon\to 0}\frac{1}{\varepsilon}\left[-X(\omega)+\exp(i\omega\varepsilon)X(\omega)\right] = X(\omega)\lim_{\varepsilon\to 0}\frac{1}{\varepsilon}\left[\exp(i\omega\varepsilon)-1\right] \\
&= X(\omega)\lim_{\varepsilon\to 0}\frac{1}{\varepsilon}\left[\sum_{n=0}^{\infty}\frac{(i\omega)^n\varepsilon^n}{n!}-1\right] \\
&= X(\omega)\lim_{\varepsilon\to 0}\frac{1}{\varepsilon}\sum_{n=1}^{\infty}\frac{(i\omega)^n\varepsilon^n}{n!} = X(\omega)\lim_{\varepsilon\to 0}\left[i\omega+\sum_{n=2}^{\infty}\frac{(i\omega)^n\varepsilon^{n-1}}{n!}\right] = i\omega X(\omega)
\end{aligned} \quad . \tag{D.5}$$

Using the algebraic properties of the Fourier transform, we get from Eqs. (D.3) and (D.4) an equation for P_y and equations for M_{nx} and M_{nz}.

$$\partial_{tt}P_y+\Gamma_e\partial_t P_y=\varepsilon_0\omega_{pe}^2E_y\,, \tag{D.6}$$

$$\partial_{tt}M_{nx}+\Gamma_m\partial_t M_{nx}=\mu_0\omega_{pm}^2H_x \quad M_{nx}=\frac{1}{\mu_0}M_x \text{ “normalized magnetization,”} \tag{D.7}$$

and

$$\partial_{tt}M_{nz}+\Gamma_m\partial_t M_{nz}=\mu_0\omega_{pm}^2H_z \quad M_{nz}=\frac{1}{\mu_0}M_z \text{ “normalized magnetization.”} \tag{D.8}$$

Defining new variables, we get the first order system

$$K_x=\partial_t M_{nx}$$

$$K_z=\partial_t M_{nz}$$

$$J_y=\partial_t P_y\,.$$

Combining the time-domain expressions for the currents expressed in terms of these new variables with Maxwell’s equations gives

$$\begin{aligned}
\nabla\times\mathbf{E} &= -\mu_0\partial_t\mathbf{H}-\mathbf{M} \\
\nabla\times\mathbf{H} &= \varepsilon_0\partial_t\mathbf{E}+\mathbf{P}
\end{aligned} \tag{D.9}$$

and yields scalar equations for the reduced, two-dimensional (2D) simulation:

$$\partial_t H_x = \frac{1}{\mu_0}\left(\partial_z E_y - K_x\right), \tag{D.10.1}$$

$$\partial_t K_x = \mu_0 \omega_{pm}^2 H_x - \Gamma_m K_x, \tag{D.10.2}$$

$$\partial_t H_z = -\frac{1}{\mu_0}\left(\partial_x E_y + K_z\right), \tag{D.10.3}$$

$$\partial_t K_z = \mu_0 \omega_{pm}^2 H_z - \Gamma_m K_z, \tag{D.10.4}$$

$$\partial_t E_y = \frac{1}{\varepsilon_0}\left[\left(\partial_z H_x - \partial_x H_z\right) - J_y\right], \tag{D.10.5}$$

and

$$\partial_t J_y = \varepsilon_0 \omega_{pe}^2 E_y - \Gamma_e J_y. \tag{D.10.6}$$

We next form the discretized versions of Eq. (D.10) to get

$$H_x^{t+1}(i,j) = H_x^t(i,j) + \frac{\delta_t}{\mu_0}\left[\frac{1}{\delta_z}\left(E_y^t(i,j) - E_y^t(i,j-1)\right) - K_x^t(i,j)\right], \tag{D.11.1}$$

$$K_x^{t+1}(i,j) = \left(\frac{1}{1+\frac{\delta_t}{2}\Gamma_m}\right)\left[\left(1-\frac{\delta_t}{2}\Gamma_m\right)K_x^t(i,j) + \delta_t \mu_0 \omega_{pm}^2 H_x^t(i,j)\right], \tag{D.11.2}$$

$$H_z^{t+1}(i,j) = H_z^t(i,j) - \frac{\delta_t}{\mu_0}\left[\frac{1}{\delta_x}\left(E_y^t(i,j) - E_y^t(i-1,j)\right) + K_z^t(i,j)\right], \tag{D.11.3}$$

$$K_z^{t+1}(i,j) = \left(\frac{1}{1+\frac{\delta_t}{2}\Gamma_m}\right)\left[\left(1-\frac{\delta_t}{2}\Gamma_m\right)K_z^t(i,j) + \delta_t \mu_0 \omega_{pm}^2 H_z^t(i,j)\right], \tag{D.11.4}$$

$$E_y^{t+1}(i,j) = E_y^t(i,j) + \frac{\delta_t}{\varepsilon_0}\left[\frac{1}{\delta_z}\left(H_x^t(i,j+1) - H_x^t(i,j)\right) + \frac{1}{\delta_x}\left(H_z^t(i,j) - H_z^t(i+1,j)\right) - J_y^t(i,j)\right], \tag{D.11.5}$$

and

$$J_y^{t+1}(i,j) = \left(\frac{1}{1+\frac{\delta_t}{2}\Gamma_e}\right)\left[\left(1-\frac{\delta_t}{2}\Gamma_e\right)J_y^t(i,j) + \delta_t \varepsilon_0 \omega_{pe}^2 E_y^t(i,j)\right]. \tag{D.11.6}$$

The execution of the algorithm requires the following order for optimum efficiency: (1)'->(3)'->(6)'->(5)'->(2)'->(4)'.

Figure D-1 shows the submatrix of cells participating in the calculation.

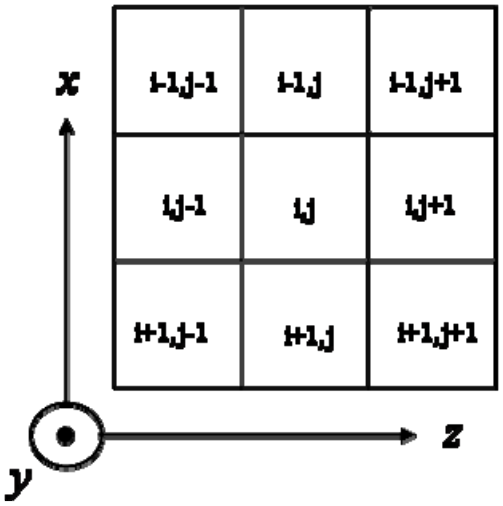

Figure D-1. Submatrix of Cells Participating in the Calculation

D.2 Absorbing Boundary Conditions

Due to finite memory limitations, computer simulations of EM fields are necessarily bounded in space. Simple conditions on the boundaries will result in the reflection of scattered waves, and the reflected waves will interfere with incident and scattered fields near the area of interest in the simulation. For most cases, this effect is undesired. In the figures below (see Figures D-2(a) and D-2(b) on page D-5)), a line source is allowed to radiate in a bounded region. At the boundaries, the first derivative of the fields is set to zero. After suitable amount of time, the radiated fields have reflected off the walls and propagating towards the source.

The simplest solution to resolve this problem, in terms of complexity, is to enlarge the simulated space. If the space is large enough, the fields in the region of interest can reach a steady-state solution before the scattered waves reach the boundary. However, enlarging the space will increase computation time considerably.

A more clever solution is to implement an Absorbing Boundary Condition (ABC) algorithm at the boundaries. As the name implies, an ABC attempts to absorb incoming scattered waves at the boundaries, hence, simulating a boundless space. The price that is paid in implementing an ABC is added code complexity and increased computation time; however, with the right ABC, the increase in computation time is not considerable.

The ABC used in our simulations is based on Liao et al. "multi-transmitting theory."[2] In Liao's ABC, the values of fields at the boundaries are approximated by extrapolating from the fields calculated inside the bounded space. More precisely, consider the function $u(x, t)$ and its discrete form uL:

$$u_L = u\,(x_{max} - L\,h,\, t - (L - 1)\,\Delta t), \tag{D.12}$$

where x_{max} is the position at the boundary and h is the spacing between elements. The value of the function at the boundary $u_0 = u(x_{max}, t + \Delta t)$ can be estimated by a polynomial extrapolation of u_L $(L > 0)$. Defining $\Delta m\, u_L = \Delta m\text{-}1\, u_L - \Delta m\text{-}1 u_L + 1$, where $\Delta 1\, u_L = u_L - u_L + 1$, an extrapolated value for u_0 of order N can be found to be

$$u_0 = u_1 + \Delta^1 u_1 + \Delta^2 u_2 + \ldots + \Delta^{N-1} u_1. \tag{D.13}$$

For N = 3 (the order used for our calculations), this simplifies to

$$u_0 = 3u_1 - 3u_2 + u_3. \tag{D.14}$$

This extrapolation method has been shown to be stable for $h = \alpha\, c\Delta t$ $0.5 < \alpha < 2$. To avoid the need for interpolation and to satisfy the finite-distance time-domain (FDTD) stability conditions, we set $\alpha = 2$. Figure D-2(a) and Figure D-2(b) show frames from computer simulations without absorbing boundaries (D-2(a)) and when the ABC algorithm is used to simulate absorbing boundaries (D-2(b)). Note the appearance of interferences from reflections in (a) but not in (b).

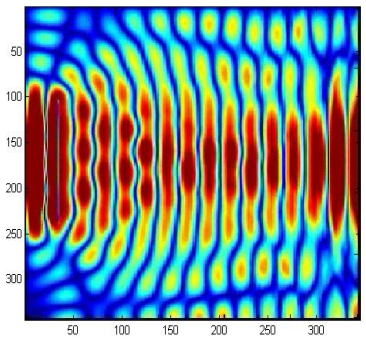

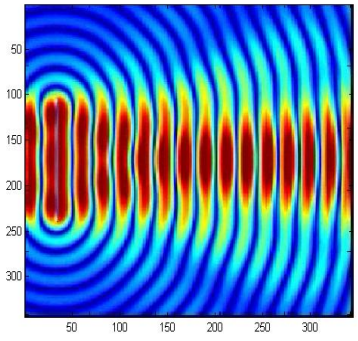

(a) **(b)**

Figure D-2. Results Without (a) and With (b) Absorbing Boundaries

2 Liao, Z. P., H. L. Wong, B. P. Yang, and Y. F. Yuan. "A Transmitting Boundary for Transient Wave Analyses." *Scientia Sinica (Series A)* 27 (10) (1984): 1063–1076.

Appendix E.
Modeling Double Negative Materials (DNMs)

E.1 Computer Code Algorithm

We developed a computer code to study wave propagation in DNMs numerically, using finite-difference time-domain (FDTD) simulations. To describe the interaction of the material with electromagnetic (EM) waves, we used a "lossy Drude model" of the medium, which is defined by a frequency dependence of the permittivity and permeability as follows:

$$\varepsilon(\omega) = \varepsilon_0\left(1 - \frac{\omega_{pe}^2}{\omega(\omega + i\Gamma_e)}\right) \tag{E.1}$$

and

$$\mu(\omega) = \mu_0\left(1 - \frac{\omega_{pm}^2}{\omega(\omega + i\Gamma_m)}\right), \tag{E.2}$$

where ω_{pe} and ω_{pm} are the electric and magnetic plasma frequency and Γ_e and Γ_m are the electric and magnetic collision frequency.

We use the following definitions to derive scalar equations for a two-dimensional (2D) simulation:

$$\partial_t H_x = \frac{1}{\mu_0}\left(\partial_z E_y - K_x\right), \tag{E.3a}$$

$$\partial_t K_x = \mu_0 \omega_{pm}^2 H_x - \Gamma_m K_x, \tag{E.3b}$$

$$\partial_t H_z = -\frac{1}{\mu_0}\left(\partial_x E_y + K_z\right), \tag{E.3c}$$

$$\partial_t K_z = \mu_0 \omega_{pm}^2 H_z - \Gamma_m K_z, \tag{E.3d}$$

$$\partial_t E_y = \frac{1}{\varepsilon_0}\left[\left(\partial_z H_x - \partial_x H_z\right) - J_y\right], \tag{E.3e}$$

and

$$\partial_t J_y = \varepsilon_0 \omega_{pe}^2 E_y - \Gamma_e J_y , \tag{E.3f}$$

which are discretized and used in the computer algorithm, as described in detail in Appendix D.

E.2 Computer Code Results

In this section, we show some simulations from our studies of normal materials *(n > 0)* and DNM *(n < 0)*. These are frames from movies that run from the time the source is turned on until a pre-selected time. See Appendix A for movie samples (p. A-29 and A-30).

Figure E-1(a) shows the result of a simulation of a wave propagating through a rectangular slab with parallel sides made of normal material. For comparison, Figure E-1(b), shows a wave propagating through a rectangular slab made of DNM. In (a), the phase velocity is parallel to the group velocity (energy flow). In (b), the two velocities are anti-parallel. Also, the wave of the normal material (Figure E-1(a)) is spreading out while the wave of the DNM (Figure E-1(b)) is focusing.

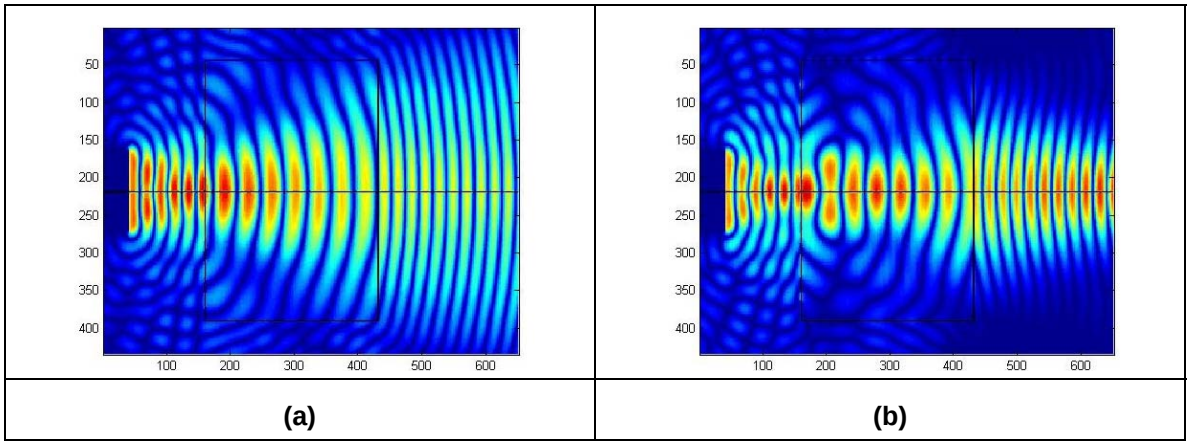

Figure E-1. Propagation Through a Rectangular Slab (Prism) Made of Normal Material (a) and DNM (b)

In Figure E-2(a) and E-2(b), the same comparison is made for a trapezoidal slab. Here, however, the negative refraction is clearly exhibited for DNM (b) as compared to the normal refraction for normal material (a) and a positive index of refraction.

The next set of figures (Figures E-3a–E-3h) show variation of refraction as a function of the index of refraction, *n*. The graph on the right of each figure shows the assumed *n*—a vertical line in the figure intersecting the *n* curve.

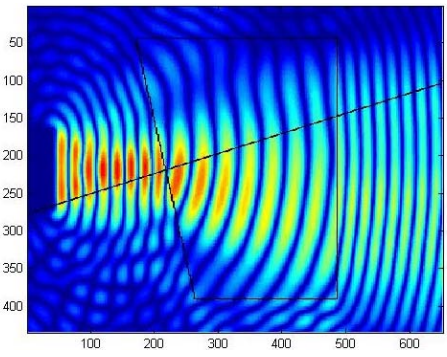

(a)

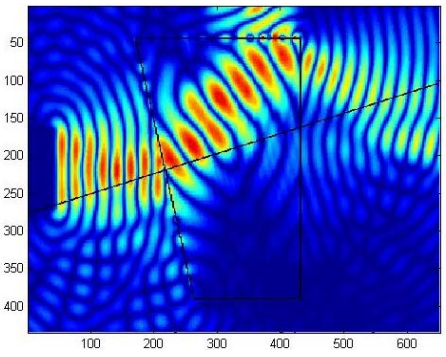

(b)

Figure E-2. Propagation Through a Trapezoidal Slab (Prism) Made of Normal Material (a) and DNM (b)

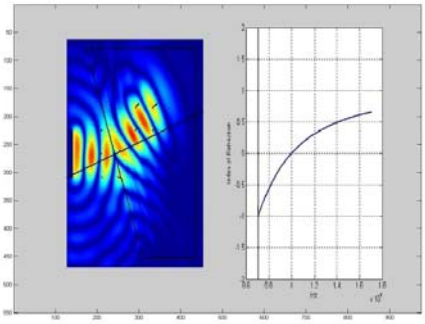

(a)

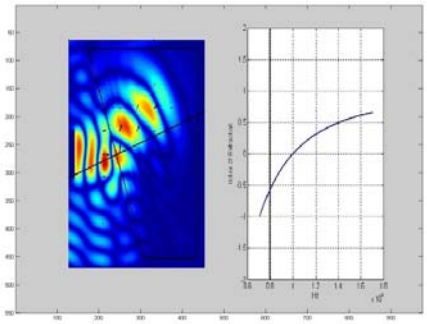

(b)

Figure E-3. Refraction of an EM Beam as It Passes From Air Into Materials With Different Index, *n*

Note 1 for Figure E-3: *In (a), n = –1; in (b), n = –0.5*

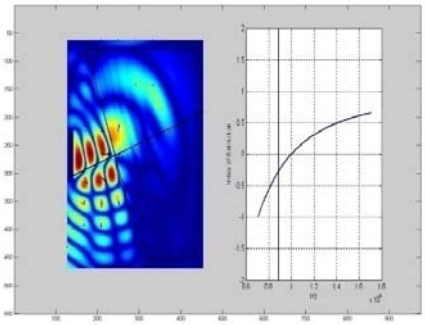

(c)

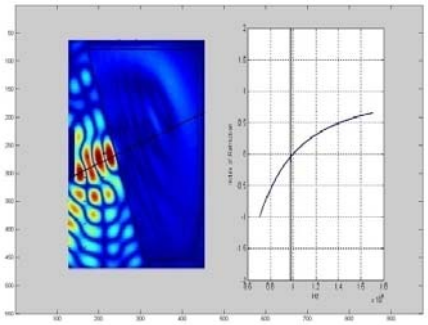

(d)

Figure E-3. Refraction of an EM Beam as It Passes From Air Into Materials With Different Index, *n*

Note 2 Figure E-3: *In (c), n = –0.25; in (d), n = 0*

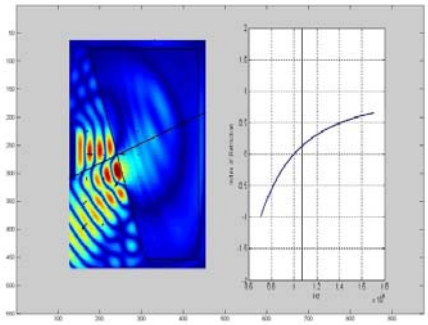	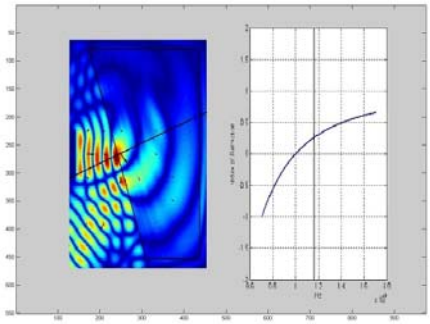
(e)	**(f)**

Figure E-5. Refraction of an EM Beam
as It Passes From Air Into Materials With Different Index, *n*

Note 3 for Figure E-3: *In (e), n = 0.1; in (f), n = 0.25*

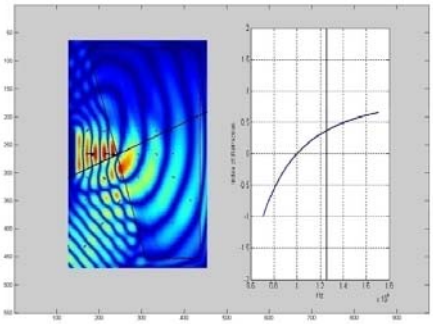	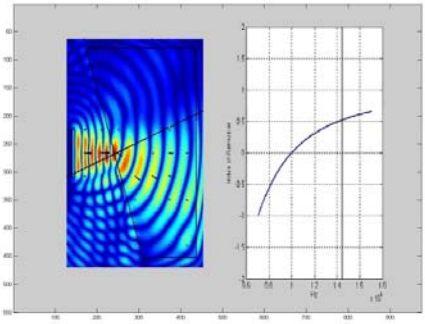
(g)	**(h)**

Figure E-3. Refraction of an EM Beam
as It Passes From Air Into Materials With Different Index, *n*

Note 4 for Figure E-3: *In (g), n = 0.4; in (h), n = 0.5*

Appendix F.
Metamaterial Applications

F.1 Phase Compensation

Since phase velocity is anti-parallel with the group velocity, a double-negative (DNG) metamaterial can be used for phase compensation. The example given in Engheta and Ziolkowski[1] considers a wave traveling through a double-positive (DPS) (normal) material of thickness *d1* and index of refraction *n1*. The wave will accumulate a relative phase difference after traveling through the material dependent on *n1* and *d1*

$$n1*k*d1, \tag{F.1}$$

where *k* is the wave number.

If the wave subsequently travels through a DNG material of thickness *d2* and index of refraction $n2 = -|n2|$, the total phase difference is

$$k*(n1*d1 - |n2|*d2). \tag{F.2}$$

Therefore, the phase difference can be eliminated by a proper choice of *n2* and *d2*.

F.2 Dispersion Compensation in Transmission Line

Metamaterials can be used to compensate for the dispersion of signals in transmission lines. Essentially, this involves choosing ε and μ such that the combination of the uncompensated transmission line channel and the metamaterial compensator gives an effective index of refraction equal to 1.

F.3 Subwavelength Focusing

This is essentially the perfect lens effect proposed by Pendry[2] and is already discussed in the report.

---

1 Engheta, N., and R. W. Ziolkowski, eds. Electromagnetic Materials: Physics and Engineering Explorations. (New Jersey: John Wiley and Sons IEEE Press, 2006).

2 Pendry, J. B. "Negative Refraction Makes a Perfect Lens." *Phys. Rev. Lett.* 85 (18) (2000): 3966–3969.

F.4 Zero Index of Refraction

Construction of metamaterials that have small index-of-refraction values has been reported. Some researchers claim that a zero-index material can be used to produce extremely narrow antenna patterns.

Another example, which is discussed in Engheta and Ziolkowski,[3] considers an infinite zero-index cylinder with a line current and surrounded by vacuum. The solution to Maxwell's equations gives a spatially static electric field inside the cylinder and an oscillatory solution outside. Even though the electric field is static inside, waves propagate from the cylinder into space.

F.5 Subwavelength Cavities and Waveguides

Generally, the size and geometry of a waveguide determine the modes (frequencies) allowed to propagate inside. Also, in normal waveguides, the size of the system forces a frequency cutoff below which modes cannot propagate. If the waveguide is filled with a composite DPS/DNG material, the cutoff frequency can be lowered or even removed without changing the overall size of the waveguide. Also, for certain geometries, waveguides can be made with metamaterials to have only one allowed propagating mode.

F.6 Resonant Enhancement of Source Generated Fields

Clever combinations of DNG or single-negative (SNG) materials with DPS materials can create channels that have an effective impedance close to zero. Such small impedance would give large enhancement of source emitted fields.

F.7 Efficient, Electrically Small Dipole Antennas

For dipole antennas surrounded by DPS materials (or free space), the radiation efficiency of the antenna decreases significantly with size. However, according to researchers, if the antenna is instead surrounded by a well-chosen DNG shell, the efficiency can be dramatically increased.

F.8 Artificial Magnetic Conductor (AMC)

Metamaterials can be constructed with low permitivities and large permeabilities. Such materials can be considered as artificial magnetic conductors. Incident waves on

---

[3] Engheta, N., and R. W. Ziolkowski, eds. Electromagnetic Materials: Physics and Engineering Explorations. (New Jersey: John Wiley and Sons IEEE Press, 2006).

perfect AMCs would have zero-phase reflection. AMCs can be used to resonantly enhance fields radiated from simple antennas.

F.9 Beam-Squinting Reduction in Series Fed Antenna Arrays

Antenna arrays typically require each element to be fed with signals in phase, and makes use of phase-compensated transmission lines. The phase compensation is frequency dependent, so a change in operating frequency leads to phase mismatching among the antenna elements, resulting in squinted beam patterns. Theoretically, this hurdle can be overcome by using negative index of refraction (NIR) transmission lines for phase compensation. In theory, this phase compensation is not frequency dependent, and, therefore, beam squinting is reduced.

F.10 Backward Leaky-Wave Antenna

Some antennas couple power in small increments per unit length, either continuously or discretely, from a traveling wave structure to free space. One example is a leaky-wave antenna that radiates microwave and millimeter-wave energy from a series of metal strips mounted on a dielectric waveguide that operates similarly to an optical fiber. The spacing of the metal strips relative to the guided wavelength determines the direction of radiation. Leaky-wave antennas are inexpensive and easy to fabricate, which makes them attractive for millimeter-wave systems. In the backward leaky wave antenna, the wave propagates away from the antenna, but the radiation propagates away from the surface at some angle. In the forward leaky wave antenna, the radiation is in the forward direction. The angle of radiation depends on the phase matching at the surface.

Applications of leaky-wave metamaterials include tunable antennas, beam-forming structures, inexpensive complex conventional phased arrays, compact-range wave generation and measurements, and endfire antennas.

F.11 Resonance Cone Antennas

A planar wire-grid network loaded with closely spaced orthogonal capacitors and inductors is the metamaterial used in the resonance cone antenna. It is positioned over a ground plane parallel to the plane. It is exited by a single-frequency point source and exhibits conical high-field regions (hence, the name). When two such metamaterials are interfaced, the cones exhibit negative refraction as well as subwavelength focusing.

Applications might include instantaneous spectrum analyzers or antenna multiplexers.

F.12 Filters and Diplexers (Microwave)

The resonance features of DNG materials make them suitable for a wide range of filter and frequency multiplexing applications. However, losses and asymmetric frequency responses are still hurdles for this type of application.

F.13 Tunable Transmission Lines

Transmission lines made from metamaterials are more tunable than their typical counterparts—which allows the construction of transmission lines of greater functionality.

REPORT DOCUMENTATION PAGE

Form Approved
OMB No. 0704-0188

1. REPORT DATE	2. REPORT TYPE	3. DATES COVERED *(From–To)*
July 2009	Final	November 2007 – July 2009

4. TITLE AND SUBTITLE

Double Negative Materials (DNM),
Phenomena and Applications

5a. CONTRACT NUMBER
DASW01 04 C 0003

5b. GRANT NUMBER

5c. PROGRAM ELEMENT NUMBER

6. AUTHOR(S)

John Franklin
John Biddle
Bohdan Balko

5d. PROJECT NUMBER

5e. TASK NUMBER
CRP 2117

5f. WORK UNIT NUMBER

7. PERFORMING ORGANIZATION NAME(S) AND ADDRESS(ES)

Institute for Defense Analyses
4850 Mark Center Drive
Alexandria, VA 22311-1882

8. PERFORMING ORGANIZATION REPORT NUMBER

IDA Document D-3887
Log: H09-000915

9. SPONSORING / MONITORING AGENCY NAME(S) AND ADDRESS(ES)

Institute for Defense Analyses
4850 Mark Center Drive
Alexandria, VA 22311-1882

10. SPONSOR/MONITOR'S ACRONYM(S)

11. SPONSOR/MONITOR'S REPORT NUMBER(S)

12. DISTRIBUTION/AVAILABILITY STATEMENT

Approved for public release; distribution is unlimited. (27 October 2009)

13. SUPPLEMENTARY NOTES

14. ABSTRACT

In this document we examine recent developments in double negative materials (DNM) or negative index of refraction materials (NIR) and consider their potential military applications. These materials are artificially engineered, composite structures that provide extraordinary responses to electromagnetic (EM) waves in general. These materials are important because they allow us to control light (or EM waves) in ways not previously possible. Because these metamaterials exhibit a unique ability to bend and focus light in ways no other conventional materials can, they hold great potential for enabling a number of innovative lens and antenna structures. Searching for smaller, lighter, and conformal components and devices for radar and communication applications, researchers have increasingly turned to these metamaterials. It is expected that research will lead to innovative designs in optical instrumentation, sub wavelength resolution, reduction of friction in MEMS, novel approaches to beam steering, novel approaches for integrating optics with semiconductor electronics and others. Many IDA projects could benefit from the knowledge obtained as a result of this study.

15. SUBJECT TERMS

Negative Index Material, Double Negative Material

16. SECURITY CLASSIFICATION OF:			17. LIMITATION OF ABSTRACT	18. NUMBER OF PAGES	19a. NAME OF RESPONSIBLE PERSON
a. REPORT	b. ABSTRACT	c. THIS PAGE			Philip L. Major
Uncl.	Uncl.	Uncl.	SAR	70	19b. TELEPHONE NUMBER *(include area code)* 703-845-2201

Standard Form 298 (Rev. 8-98)
Prescribed by ANSI Std. Z39.18

The Institute for Defense Analyses is a non-profit corporation that administers three federally funded research and development centers to provide objective analyses of national security issues, particularly those requiring scientific and technical expertise, and conduct related research on other national challenges.